Politecnico di Torino

Laurea Magistrale in Mechanical Engineering

Anno accademico: 2020/2021

Sessione di Laurea: Luglio 2021

Performance Study of the Three-Piece and Y25 Bogies Using Frenet Geometric Analysis

Relatori:

Nicola Bosso, Politecnico di Torino

Nicolò Zampieri, Politecnico di Torino

Ahmed A. Shabana, University of Illinois at Chicago

Candidato:

Dario Bettamin

PREMESSA

Questo elaborato è il frutto di un'esperienza di ricerca condotta negli Stati Uniti presso il dipartimento di Ingegneria Meccanica dell'Università dell'Illinois a Chicago ed è basato sull'articolo "Frenet Performance Evaluation of Railroad Vehicle Systems", accettato per la pubblicazione dalla rivista scientifica Acta Mechanica (Bettamin et al, 2021). La tesi riporta uno studio comparativo tra due carrelli ferroviari molto usati nei treni merci: il *carrello three-piece*, diffuso in Nord America e altre parti del mondo, e il *carrello Y25*, diffuso in Europa. I parametri di confronto si basano su un approccio innovativo fondato sull'integrazione di formulazioni *multibody* non lineari tramite computer software e nuovi concetti geometrici non comuni in letteratura. Gli algoritmi multibody sono utilizzati per generare e risolvere numericamente equazioni differenziali/algebriche in modo automatico, così da determinare le *traiettorie reali del moto* dei carrelli. Per avere una migliore comprensione del comportamento dinamico dei veicoli, viene fatta una distinzione tra la traiettoria reale da essi tracciata e la geometria dei binari. Le traiettorie reali sono descritte usando gli angoli di Frenet-Eulero, che sono dipendenti dal moto e differiscono dagli angoli che entrano nella definizione della geometria della traccia. In particolare, il *Frenet bank angle* definisce la sopraelevazione del piano del moto, che contiene la traiettoria reale e varia durante il movimento del veicolo, a differenza dell'angolo di inclinazione della traccia, che rimane costante. In questa tesi è spiegata la differenza tra l'equilibrio delle forze laterali calcolato nel piano della traccia e quello calcolato nel piano di Frenet, basato sulle traiettorie reali. Sono state eseguite simulazioni delle performance dei carrelli su una traccia curva e i risultati numerici ottenuti vengono qui presentati, con particolare attenzione data alle deviazioni della traiettoria reale rispetto alla linea centrale tra i binari. Poiché non è possibile includere in un unico studio tutti i parametri di valutazione dei carrelli, questa ricerca è incentrata sull'analisi dell'angolo di attacco, delle forze di contatto tra flange e binari e delle forze centrifughe agenti sui due carrelli. I risultati vengono presentati senza fornire un giudizio sulle prestazioni complessive dei veicoli.

Dedicated to the memory of my mother.

AKNOWLEDGEMENTS

Firstly, I would like to thank my father, who convinced me to join the international program I took part at the University of Illinois and supported me during this project. Without him this research would not have been possible. I would also like to thank my advisors and my laboratory mates, who instructed and helped me during my work. I also thank the friends who shared with me this incredible experience in Chicago and made it unforgettable. Last but not least, I thank my girlfriend, who always supported me despite the distance that divided us and encouraged me when needed, with patience and love.

DB

CONTRIBUTIONS OF AUTHORS

Professor Ahmed A. Shabana, my advisor from University of Illinois at Chicago, provided the simulation software used in this investigation and contributed to the development of the formulation used. He also supervised the research, helped in the thesis writing and edited some chapters. Professors Nicola Bosso and Nicolò Zampieri, my advisors from Politecnico di Torino, provided me some important material for the construction of bogies models, in particular for the selection of simulation data for the Y25 bogie model. All my advisors contributed in the thesis revision and final adjustments.

TABLE OF CONTENTS

TABLE OF CONTENTS (continued)

LIST OF TABLES

TABLE **PAGE**

LIST OF FIGURES

LIST OF ABBREVIATIONS

DDS	Data-Driven Science
MBS	Multibody System
DAE	Differential/Algebraic Equation
AMT	Actual Motion Trajectory
UIC	International Union of Railways
ORE	Office de Recherches et d’Essais
APTA	American Public Transportation Association
SIGMA/SAMS	Systematic Integration of Geometric Modeling and Analysis for the Simulation of Articulated Mechanical Systems
AREMA	American Railway Engineering and Maintenance-of-Way Association
EN	European Norm
ANCF	Absolute Nodal Coordinate Formulation
AAR	Association of American Railroads
BR	British Rail
BS	British Standard

SUMMARY

In this thesis, a *data-driven science* (DDS) approach, based on integrating nonlinear *multibody system* (MBS) formulations and new geometric concepts, is used to compare the performance of two widely used railroad bogies: the *three-piece bogie*, widely used in North America and other parts of the world, and the European *Y25 bogie*. Despite their popularity, such a comparative study, based on a MBS approach, is lacking in the literature. MBS algorithms are used to automatically construct and numerically solve the bogie nonlinear differential/algebraic equations (DAEs) to determine the bogie motion trajectories. To have a better understanding of the bogie dynamic behavior, new criteria are used in the comparative study performed in this investigation. To this end, a distinction is made between geometry of *actual motion trajectories* (AMT) and the track geometry. The AMT curves are described using the motion-dependent Frenet-Euler angles, referred to as Frenet bank, curvature, and vertical development angles, which differ from their counterparts used in the description of the track geometry. In particular, the Frenet bank angle defines the super-elevation of the AMT curve *osculating plane*, referred to as the *motion plane*, which changes with time as the vehicle moves, distinguished from the fixed-in-time track super-elevation. This thesis explains the difference between the *lateral track plane force balance* used in practice to determine the balance speed and the *Frenet force balance* which is based on recorded motion trajectories. Computer simulations of bogies travelling on track, consisting of tangent, spiral, and curve sections, are performed with particular attention given to the deviations of the AMT curves from the track centerline. The results obtained in this study demonstrate the dependence of the AMT curve geometry on the wheelset forward motion, highlighting the limitations of tests performed using roller test rigs which do not allow longitudinal wheelset motion. Because all bogie performance criteria cannot be addressed in

one study, this investigation is focused on recording *centrifugal inertia forces* of the two bogie types without making judgement on their overall performance. The contents of this thesis are based on the paper “Frenet Performance Evaluation of Railroad Vehicle Systems”, accepted for publication by the journal Acta Mechanica (Bettamin et al, 2021).

CHAPTER 1

INTRODUCTION

Freight rail transportation is considered four times more efficient and more environmentally friendly compared to highway transportation (Cuenot and Gabriel, 2016). To enhance the performance and safety of rail transportation, railroad vehicle dynamics and stability have been the subject of a large number of investigations (Andersson and Abrahamsson, 2002; Berghuvud, 2002; De Pater, 1988; Elkins and Gostling, 1977; Endlicher and Lugner, 1990; Grassie, 1993; Handoko et al, 2020; Kik, 1992; Knothe and Grassie, 1993; Knothe and Stichel, 1994; Pascal and Sany, 2019; True, 1994). In particular, railroad vehicle derailments, which received special attention, remain common, including the ones resulting from wheel climb at relatively low speeds. Nonetheless, derailment criteria failed to provide explanation of many accidents with causes relevant to the analysis of this study due to several reasons: (1) Some of the derailment criteria are based on simplified approaches that do not take into account the three-dimensional nature of the forces that lead to wheel climb; (2) Lack of proper interpretation of the wheelset forces including inertia forces; and (3) Misinterpretation of the role of the track geometry and its influence on the vehicle dynamics. Because of the railroad wheel conicity, the simplest motion of a wheelset is three-dimensional, and consequently, use of three-dimensional force analysis is necessary with or without large angles of attack. Planar force equilibrium can lead to simplifications that ignore the complex nature of three-dimensional dynamics of railroad vehicles. Because of the complexity of rail car dynamics and the wheel/rail interaction forces, analytical models and linearization techniques are not adequate for accurately capturing the rail vehicle dynamics. For this reason, computer simulations based on nonlinear formulations are necessary in order to account for model details that cannot be included when using simplified approaches or linearization techniques.

The lack of proper interpretation of the forces that influence the motion of the railroad vehicle is another factor that has contributed to limiting the effectiveness of existing derailment criteria considered for serious accident investigations. Even in the case of a tangent (straight) track, the lateral inertia force due to the hunting oscillations can be significant. This lateral force, which can be interpreted as a centrifugal inertia force, can exert very high force on the track structure if it is not properly balanced (Shabana, 2021). During hunting oscillations on a tangent track, centers of mass of vehicle components trace space curves that have their own geometric characteristics. Curve motion, regardless of the track geometry, produces centrifugal inertia forces that can have significant lateral component, particularly at the peaks of the hunting oscillations. The magnitude of such a lateral centrifugal force component increases in case of heavier vehicles operating at relatively higher speeds. The actual motion trajectories can be sharp curves with large curvatures and small radii of curvature, much smaller than the *minimum curve radius* mandated in North America by federal regulations when constructing the track geometry. Therefore, recorded motion trajectories obtained from computer simulations can be used effectively to shed light on the behavior of the vehicle if the forces are properly interpreted.

Another important fact often overlooked in the study of railroad vehicle systems is the role of the *track geometry* and its influence on the motion trajectories. For example, track super-elevations are used to create a lateral component of the gravity force to balance the lateral component of the centrifugal inertia force. This force balance is used to define a *balance speed* recommended for the vehicle safe operation during curve negotiations. In defining the balance speed, it is assumed that the rail car strictly traces a circular curve that lies in a plane parallel to the horizontal plane. Because of this assumption, which is violated in most practical motion scenarios, the centrifugal inertia force is assumed to lie in a plane parallel to the horizontal plane. Nonetheless, observations confirm that the gravity/centrifugal force balance is not totally effective in eliminating the lateral motion, and as a consequence, the rail car often slides toward the high and low rails, exerting significant lateral force on the track structure. Clearly, the assumption of a horizontal centrifugal inertia force may be satisfied if the wheel flanges remain in continuous contact with a constant curve section of a rail, which is an undesirable motion scenario because of the possible high contact force and wheel climb. A vehicle that traces a short straight line on a super-elevated track does not have a centrifugal inertia force during this short travel, demonstrating the importance of proper distinguishing between the geometry of the motion trajectories and the track geometry. The recorded motion trajectories define accurately the vehicle motion and provide proper interpretation of the forces.

The above discussion explains the importance of the motion and geometry concepts in the performance evaluation of railroad vehicle systems. In this investigation, a *data-driven science* (DDS) approach that integrates nonlinear computational *multibody system* (MBS) formulations and new geometric concepts and interpretations, is used to compare the performance of two bogies widely used in North America, Europe, and other parts of the world. These bogies are the *three-piece bogie*, widely used in North America and other parts of the world, and the European *Y25 bogie*. This study addresses an obvious lack of a meaningful three-piece/Y25 bogie comparative study based on a nonlinear MBS approach and proper interpretation of the geometry and forces. MBS algorithms are used to automatically construct and numerically solve the bogie nonlinear differential/algebraic equations (DAEs) and record motion trajectories that define the system dynamics (Ginsberg, 2008; Goldstein, 1950; Greenwood, 1988; Huston, 1990; Roberson and Schwertassek, 1988; Shabana, 2021). New criteria are used in the comparative study performed in this investigation, based on distinguishing between geometry of *actual motion trajectories* (AMT) and track geometry. The AMT curves are described using the motion-dependent Frenet bank, curvature, and vertical development angles, which differ from their counterparts used in the description of the fixed-in-time track geometry. Distinction is also made between the *osculating plane*, referred to as the *motion plane*, and the *track plane* (Do Carmo, 2016; Farin, 1999; Gallier, 2011; Goetz, 1970; Kreyszig, 1991; Piegl and Tiller, 1997; Rogers, 2001). The motion plane is formed by the two vectors tangent and normal to the AMT curves, while the track plane is defined by the value of the track curvature, vertical development, and bank angles. The Frenet bank angle defines the super-elevation of the AMT curve osculating plane (motion plane), which changes with time as the vehicle moves, while the track super-elevation is motion independent (Ling and Shabana, 2021; Shabana and Ling, 2021). In this study, particular attention is given to the deviations of the AMT curves from the track centerline curve. These deviations are measures of the violation of the lateral force balance used to define the balance speed currently used in practice, and demonstrate the importance of the concept of the *Frenet force balance* which is based on recorded motion trajectories. It is shown analytically in this study that as the Frenet bank angle increases, the component of the gravity force which can balance the centrifugal force in its totality also increases. Computer simulations of the two bogies during curve and tangent track negotiations are conducted and the results are presented to compare the three-piece and Y25 bogie performance in specific areas without making a general judgement on the overall bogie performance, which requires several focused future investigations. Nonetheless, the analysis presented in this investigation, based on the recorded motion trajectories, explains limitations of using *scaled roller rigs* in the prediction of the forces that influence the wheelset and bogie dynamics. The motion trajectories are greatly influenced by the forward motion, and therefore, force interpretation using testing of wheelsets that do not move longitudinally can lead to wrong prediction of the inertia forces as well as the contact forces.

CHAPTER 2

PERFORMANCE MEASURES AND MOTION TRAJECTORIES

The DDS approach used in this investigation to compare the performance of the three-piece and the Y25 bogies is based on recording the motion trajectories using nonlinear MBS computer algorithms, which allow for including model details that are not captured using simplified approaches or linearization techniques. The recorded motion trajectories can be used to accurately determine the centrifugal inertia forces and the time-variant *Frenet bank angle*, which differs from the time-invariant track bank angle. The results of the centrifugal force and Frenet bank angle predicted for the two bogies under the same simulation conditions are compared. The details, components, and structures of the three-piece and Y25 bogies will be described in a later chapter of this thesis.

2.1 Recorded Motion Trajectories

By performing computer simulations, the global position vectors of the bogie components can be recorded to define motion trajectory space curves used to extract the information required to compare the performance of the three-piece and Y25 bogies in specific areas. For a component i of the bogie system, the space curve $\mathbf{r}^i = \begin{bmatrix} x^i & y^i & z^i \end{bmatrix}^T = \mathbf{r}^i(t)$ that defines the global position of the component mass center, the absolute velocity vector $\dot{\mathbf{r}}^i = \dot{\mathbf{r}}^i(t)$, and the absolute acceleration vector $\ddot{\mathbf{r}}^i = \ddot{\mathbf{r}}^i(t)$ can be recorded. The velocity vector can be written as $\dot{\mathbf{r}}^i(t) = \dot{s}\mathbf{r}_s^i$, where $\dot{s} = \left|\dot{\mathbf{r}}^i\right|$ is the magnitude of the velocity along the unit tangent vector $\mathbf{r}_s^i = \partial\mathbf{r}^i/\partial s$, and s is the arc length of the curve $\mathbf{r}^i = \mathbf{r}^i(t)$. The arc length s of the recorded motion trajectory should be distinguished from the arc length used to describe the track centerline and the right and left rail space curves. That is, the velocity vector recorded as function of time can be used to determine the magnitude of the velocity $\dot{s}$ and the unit vector $\mathbf{r}_s^i = \partial \mathbf{r}^i / \partial s$ tangent to the curve. The recorded velocity vector can also be used to determine the partial derivative of the vector $\mathbf{r}^i$ with respect to any of the coordinates x^i, y^i and z^i by using the relationship $\dot{\mathbf{r}}^i = \mathbf{r}_\alpha^i \dot{\alpha}^i$, $\alpha^i = x^i, y^i, z^i$, where $\mathbf{r}_\alpha^i = \partial \mathbf{r}^i / \partial \alpha^i$, provided that $\dot{\alpha}^i \neq 0$. For example, if $\dot{y}^i \neq 0$, $\mathbf{r}_y^i = \partial \mathbf{r}^i / \partial y^i = \dot{\mathbf{r}}^i / \dot{y}^i$. The arc length of the motion trajectory curve can also be determined by numerically integrating the differential relationship $ds = \dot{s} dt$.

2.2 Centrifugal Forces

The centrifugal force does not appear in the Newton-Euler equations of rigid bodies that negotiate curves. The recorded motion trajectories can be used to conveniently define the centrifugal force vector. To this end, the absolute velocity vector $\dot{\mathbf{r}}^i(t) = \dot{s}\mathbf{r}_s^i$ is differentiated with respect to time to obtain the absolute acceleration vector $\ddot{\mathbf{r}}^i(t) = \ddot{s}\mathbf{r}_s^i + (\dot{s})^2 \mathbf{r}_{ss}^i$. This equation can be written as $\ddot{\mathbf{r}}^i(t) = \ddot{s}\mathbf{r}_s^i + \left((\dot{s})^2 / R\right)\mathbf{n}^i$, where $R = 1/\kappa$ is the radius of curvature, $\kappa = \left|\mathbf{r}_{ss}^i\right|$ is the curve curvature, and $\mathbf{n}^i = \mathbf{r}_{ss}^i / \left|\mathbf{r}_{ss}^i\right|$ is the unit vector normal to the motion trajectory curve of the component i. Because $\mathbf{r}_s^i$ and $\mathbf{n}^i$ are two orthogonal unit vectors and $\ddot{\mathbf{r}}^i$ is recorded, the dot product of $\mathbf{r}_s^i$ and the acceleration vector $\ddot{\mathbf{r}}^i(t) = \ddot{s}\mathbf{r}_s^i + \left((\dot{s})^2 / R\right)\mathbf{n}^i$ can be used to determine $\ddot{s}$ as $\ddot{s} = \mathbf{r}_s^i \cdot \ddot{\mathbf{r}}^i(t)$. Therefore, the centrifugal inertia force vector is defined as

$$\mathbf{F}_{ic}^i = m^i \left((\dot{s})^2 / R\right)\mathbf{n}^i = m^i \left(\ddot{\mathbf{r}}^i(t) - \ddot{s}\mathbf{r}_s^i\right) \tag{1}$$

where m^i is the mass of the bogie component. The centrifugal inertia force determined using the recorded motion trajectory procedure described in this chapter will be used to compare the performance of the three-piece and Y25 bogies. As will be discussed, there can be significant centrifugal inertia forces not only during negotiation of super-elevated curved track, but also during negotiation of tangent (straight) track because of the non-zero curvature of the motion trajectory curves during the hunting oscillations. Another performance measure that will be used in this study is the Frenet bank angle described in the following chapter, after the brief discussion of the MBS approach used to determine the recorded motion trajectories. The Frenet bank angle defines the correct direction of the centrifugal force.

2.3 MBS Approach

The recorded motion trajectories are obtained using a nonlinear MBS formulation that allows for modeling mechanical joints as well as bushing and friction elements. The spatial motion of a rigid body is described using six generalized coordinates, three translational and three rotational. The global position of a point on a body i is defined as $\mathbf{r}^i = \mathbf{R}^i + \mathbf{u}^i = \mathbf{R}^i + \mathbf{A}^i \bar{\mathbf{u}}^i$, where $\mathbf{R}^i$ is the global position vector of the origin of the body coordinate system, $\mathbf{A}^i$ is the transformation matrix that defines the body orientation in the global coordinate system, and $\mathbf{u}^i$ and $\bar{\mathbf{u}}^i$ are the local position vectors of the point defined in the global and body coordinate systems, respectively (Shabana, 2020). The absolute velocity vector of the arbitrary point is $\dot{\mathbf{r}}^i = \dot{\mathbf{R}}^i + \boldsymbol{\omega}^i \times \mathbf{u}^i = \dot{\mathbf{R}}^i + \mathbf{A}^i \left(\bar{\boldsymbol{\omega}}^i \times \bar{\mathbf{u}}^i \right)$, where $\boldsymbol{\omega}^i$ and $\bar{\boldsymbol{\omega}}^i$ are the absolute angular velocity vectors defined in the global and the local coordinate systems, respectively. The absolute acceleration vector can be written as $\ddot{\mathbf{r}}^i = \ddot{\mathbf{R}}^i + \left(\boldsymbol{\alpha}^i \times \mathbf{u}^i \right) + \boldsymbol{\omega}^i \times \left(\boldsymbol{\omega}^i \times \mathbf{u}^i \right)$, or $\ddot{\mathbf{r}}^i = \ddot{\mathbf{R}}^i + \mathbf{A}^i \left(\bar{\boldsymbol{\alpha}}^i \times \bar{\mathbf{u}}^i \right) + \mathbf{A}^i \left(\bar{\boldsymbol{\omega}}^i \times \left(\bar{\boldsymbol{\omega}}^i \times \bar{\mathbf{u}}^i \right) \right)$, where $\boldsymbol{\alpha}^i$ and $\bar{\boldsymbol{\alpha}}^i$ are the angular acceleration vectors defined in the global and body coordinate systems, respectively. The velocity and acceleration vectors can be written, respectively, in terms of the four Euler parameters vector $\boldsymbol{\theta}^i$ as $\dot{\mathbf{r}}^i = \dot{\mathbf{R}}^i - \tilde{\mathbf{u}}^i \mathbf{G}^i \dot{\boldsymbol{\theta}}^i$ and $\ddot{\mathbf{r}}^i = \ddot{\mathbf{R}}^i - \tilde{\mathbf{u}}^i \mathbf{G}^i \ddot{\boldsymbol{\theta}}^i + \boldsymbol{\omega}^i \times (\boldsymbol{\omega}^i \times \mathbf{u}^i)$, where $\tilde{\mathbf{u}}^i$ is the skew symmetric matrix associated with the vector $\mathbf{u}^i$, and $\mathbf{G}^i$ is the matrix that relates the angular velocity vector to the time derivatives of Euler parameters, that is $\boldsymbol{\omega}^i = \mathbf{G}^i \dot{\boldsymbol{\theta}}^i$. Using this kinematic description, the equation of motion of the system can be written as $\mathbf{M}\ddot{\mathbf{q}} - \mathbf{Q} + \mathbf{C}_{\mathbf{q}}^T \boldsymbol{\lambda} = \mathbf{0}$, where $\mathbf{M}$ is the system mass matrix, $\mathbf{q}$ and $\mathbf{Q}$ are, respectively, the vectors of system coordinates and generalized forces, $\mathbf{C}_{\mathbf{q}}$ is the constraint Jacobian matrix, and $\boldsymbol{\lambda}$ is the vector of Lagrange multipliers. The resulting system of differential and algebraic equations (DAEs) is solved numerically to determine the motion trajectories. The algorithm for solving this DAE system is described in detail in the literature (Shabana, 2020).

CHAPTER 3

FRENET BANK ANGLE

Track super-elevations are designed to create a lateral gravity force component that balances the lateral component of the centrifugal force. While this lateral force balance is used to define the balance speed, observations of realistic motion scenarios have shown that such force balance is not always achieved leading to significant wheel/rail impact forces which can damage the track structure and lead to accidents. Furthermore, such a force balance is based on the strict assumption that the rail vehicle traces a circular curve that lies in a plane parallel to the horizontal plane, and consequently, the normal to this circular curve and the centrifugal force lie in a plane parallel to the horizontal plane. While this assumption of horizontal centrifugal force is always violated, it is to be noted that, even when using this assumption, the centrifugal force in its totality is not balanced by a component of the gravity force and such a centrifugal force has a component normal to the track in the direction of the axle load. Because the direction of the centrifugal force is not a priori known, reliance on the current definition of the balance speed without performing extensive computer simulations based on DDS approach to determine the AMT curves will not provide answers that explain the root causes of derailments.

3.1 Frenet Super-Elevation

During the vehicle motion, the centrifugal force in its totality lies in the Frenet osculating plane (motion plane) defined by the vectors tangent and normal to the AMT curve. The *Frenet bank angle* defines the motion-dependent *Frenet super-elevation* of the motion plane. This Frenet super-elevation is unique and differs from the fixed-in-time motion-independent track super-elevation. Furthermore, the non-zero Frenet bank angle and super-elevation may exist when the vehicle negotiates tangent (straight) track segments. Therefore, Frenet super-elevation, which accurately defines the direction of the centrifugal force, allows for better understanding the vehicle dynamics and the force balance during realistic motion scenarios. The uniqueness of the Frenet super-elevation also sheds light on the non-unique definition of the balance speed currently used; the track super-elevation can be increased and the balance speed can be increased accordingly giving an infinite number of choices.

3.2 Frenet-Euler Angles

The Frenet bank angle, obtained using a DDS approach, can be used as a measure to compare the performance of the three-piece and Y25 bogies. The Frenet bank angle is a measure of the amount of the Frenet super-elevation that results from the motion of different rail cars or bogies. Larger Frenet bank angle produces a larger component of the gravity force in the motion plane.

It was shown in previous investigations that the unit vectors tangent and normal to the AMT curve can be written in terms of Frenet-Euler angles, referred to for brevity as Frenet angles (Ling and Shabana, 2021; Shabana and Ling, 2021; Shabana, 2021). These Frenet angles are the *curvature angle* ψ, the *vertical development angle* θ, and the *bank angle* ϕ. In terms of these angles, the tangent and normal vectors that define the actual motion plane are defined as

$$\mathbf{r}_s = \dot{\mathbf{r}}/\dot{s} = \begin{bmatrix} x_s \\ y_s \\ z_s \end{bmatrix} = \begin{bmatrix} \cos\psi\cos\theta \\ \sin\psi\cos\theta \\ \sin\theta \end{bmatrix}, \qquad \mathbf{n} = \begin{bmatrix} -\sin\psi\cos\phi + \cos\psi\sin\theta\sin\phi \\ \cos\psi\cos\phi + \sin\psi\sin\theta\sin\phi \\ -\cos\theta\sin\phi \end{bmatrix} \tag{2}$$

where $\alpha_s = \partial\alpha/\partial s$, $\alpha = x, y, z$. Because $\mathbf{r}_s = \dot{\mathbf{r}}/\dot{s} = \begin{bmatrix} x_s & y_s & z_s \end{bmatrix}^T$ is known from the recorded trajectory data, as previously discussed, and because the unit normal $\mathbf{n} = \begin{bmatrix} n_1 & n_2 & n_3 \end{bmatrix}^T$ can be determined as the unit vector along the centrifugal force, one can determine the Frenet curvature, vertical development, and bank angles using the definitions of Equation 2 as

$$\left.\begin{aligned}
&\cos\psi = x_s \Big/ \sqrt{(x_s)^2 + (y_s)^2}, \quad \sin\psi = y_s \Big/ \sqrt{(x_s)^2 + (y_s)^2}, \\
&\cos\theta = \sqrt{(x_s)^2 + (y_s)^2}, \quad \sin\theta = z_s \\
&\cos\phi = (n_2 - y_s n_1) \Big/ \sqrt{(x_s)^2 + (y_s)^2}, \quad \sin\phi = (n_1 + y_s n_2) \Big/ z_s \sqrt{(x_s)^2 + (y_s)^2}
\end{aligned}\right\} \tag{3}$$

As discussed in the literature, use of the de l'Hopital rule ensures that the Frenet angles in the preceding equation are well defined even in the case of zero curvature (Shabana, 2021). The centrifugal force discussed in the preceding chapter and the Frenet bank angle determined in this chapter will be used in the DDS approach of this investigation as performance measures.

3.3 Gravity Force Component in the Motion Plane

It is clear from the definition of the normal vector in Equation 2 that the component of the gravity force, in the motion plane which contains the centrifugal force in its totality, is defined as

$$F_{gn} = \begin{bmatrix} 0 & 0 & -mg \end{bmatrix}^T \mathbf{n} = -mgn_3 = mg\cos\theta\sin\phi \tag{4}$$

where m is the vehicle mass and g is the gravity constant. The preceding equation shows that as the Frenet bank angle ϕ increases, the component of the gravity force that can balance the centrifugal force also increases.

CHAPTER 4

PRACTICAL CONSIDERATIONS IN BOGIE DESIGN

The bogie designs have been continuously altered and improved over a long time period that extends more than a century. The goal of the design changes has been to enhance the performance and improve the curving behavior. There are several designs that are significantly different. For example, the three-piece and Y25 bogies considered in the numerical study presented in this investigation have different structure, components, joints, and force elements. The Y25 bogie has the frame as the main part, while the three-piece bogie has the bolster and two side frames as its main structural components. In this chapter, practical bogie design considerations are presented to shed light on basic structural differences that will be further discussed when the three-piece and Y25 bogies are described in the following chapter.

4.1 Background

Developing accurate and efficient computer models for freight trains is challenging because of the large number of friction elements that can be source of problems during the numerical integration of the system equations of motion. In particular, the *friction wedge* used in the three-piece bogie and the *Lenoir link* used in the Y25 bogie are critical elements that require special attention for successful and accurate computer simulations. Developing such accurate computer models of rail vehicles is necessary because of their impact on improving the performance, efficiency, and operating cost (Kovalev et al, 2009). Previous studies have shown that freight cars equipped with three-piece bogies have increased risk of derailment as compared to the Y25 bogie (Kovalev et al, 2009; Sadeghi et al, 2011). In this investigation, computer simulations results are used to obtain recorded motion trajectories that allow extracting specific performance measures. Particular attention is given to the deviation of the recorded motion trajectory curve from the track centerline. The centrifugal force is computed using the AMT curve and new performance measures are considered, as previously discussed.

4.2 Bogie Suspension

The bogie suspension system serves as a vibration isolation that reduces the intensity of the force transmitted to the rail car. Vibrations negatively impact ride comfort in passenger trains and may damage the cargo and vehicle components of freight trains. Railroad suspensions are often arranged in different directions to absorb not only vertical vibrations but also lateral oscillations due to the wheel/rail contact forces. A suspension system consists of spring and damping elements that can have different arrangements depending on the bogie design. Rubber or air suspension systems, which are more common in passenger trains, can be used as alternatives to coil springs. Friction damping is preferred to conventional hydraulic dashpots because the dissipative damping force is proportional to the weight of the cargo.

Bogie suspension systems can have both *primary* and *secondary suspensions*. Freight cars may have only one of these suspension types: a primary suspension between the wheelsets and bogie frame, referred to as *axle box suspension*, or a secondary suspension between the bogie frame and the car body, referred to as *central suspension* (The Contact Patch, 2017). The primary suspension serves to filter out vertical high frequency vibrations and contributes to improving lateral stability of the rail vehicle. The *secondary suspension* serves as isolation of low frequency disturbances and enhances ride comfort. For this reason, secondary suspensions are more common in passenger trains than freight trains. Most passenger trains have both types of suspension to improve the stability and ride comfort.

4.3 Primary Suspension

The purpose of the primary suspension is to control the transmissibility of the high frequency wheel/rail contact forces and reduce derailment risk, vibrations, and noise (SKF, 2011). *Leaf springs*, also known as *horns*, which rest on the axle box and their ends are connected to the frame by double links attached to pins located on the underframe, were more common in the past (Railway Technical, 2004). The leaf spring suspension provides also damping as the result of friction between the spring leaves. This kind of suspension is still popular in Europe, particularly for new two-axle freight wagon applications. However, leaf spring suspensions are becoming less common in modern trains because of possible defects, particularly during braking that can lead to cracks. Furthermore, the spring elasticity can deteriorate when the spring is subjected to high pressures that cause wear of the friction surfaces (The Contact Patch, 2017). For these reasons, leaf springs are replaced by coil springs which can have different arrangements including use of two cylindrical stubs wrapped by coil springs. A collar mounted on the axle box can slide vertically on the stubs under the effect of the springs. An alternative is the rubber shear block, made of rubber enforced by steel leaves (The Contact Patch, 2017). While leaf spring problems resulting from braking are avoided when using coil springs, damping elements such as hydraulic or friction elements are needed for the energy dissipation.

4.4 Secondary Suspension

The secondary suspension, which connects the car body to the bogie frame, normally consists of a combination of air springs and rubber or metal bearers that restrict vertical, lateral, and torsional displacements (SKF, 2011). A secondary suspension system is used in most passenger trains and in few freight trains. While in the past coil springs were more common for the secondary suspension, air springs are now preferred because of their variable stiffness which make them more effective in covering a wider range of frequencies and loads. Despite their complexity and higher cost, air springs are lighter, provide better sound isolation, and their stiffness can be tuned electronically.

Freight trains may have only primary suspensions because the ride comfort is not a priority despite the fact that it is always recommended to reduce or control the vibration level. In freight trains without secondary suspensions, the car body is directly mounted on a steel plate which is supported by the primary suspension. A central pin connects the car body to the plate center to provide the rotational degree of freedom needed for safe curve negotiations. Two side bearers are placed to the right and the left of the pin to provide a stable support for the car body, which can slide on these plates while rotating (Ghazavi and Taki, 2008).

4.5 Single-Wheelset Versus Bogies

The single-wheelset running gear is mainly used for rail cars supported by two axles only. In this configuration, the rail car is mounted on two wheelsets, one on the front and one on the back. Leaf springs mounted on the axle box and connected to the car frame by two swing hangers can be used as the primary suspension, called *double-link suspension*. The axle box bearings allow the wheelset axles to rotate independently from the other components of the vehicle, while the leaf springs allow longitudinal and lateral oscillations of the axle box with respect to the car frame. The longitudinal suspension stiffness is higher than the lateral stiffness because of the leaf orientation. The leaf spring damping mechanism has advantage of being load-sensitive at the expense of exposure of the spring leaves that generate the friction to the atmosphere, dirt, and humidity that influence the spring effectiveness (Hecht, 2001). The single-wheelset running gear has been used in the past because of its simplicity, low cost, robustness, and limited space required. However, two-axle freight cars with double link suspension have poor hunting characteristics because of low level of lateral damping. Moreover, due to corrosion and wear, suspension parameters can change significantly during the vehicle life (Iwnicki, 2015). For this reason, despite single-wheelset cars are still used in Europe, current trend in industry is to use freight bogies.

While a bogie mainly consists of wheelsets, bearings, and a suspension system, it can also include a steering mechanism, brake system, lubrication devices, monitoring sensors, and other subsystems. Most modern trains are equipped with bogies containing two axles and each rail car is usually mounted on two bogies, one on the front and one on the back. Another alternative is to connect two cars using the *Jacobs design*, in which each bogie supports the ends of two consecutive cars. This configuration increases the axle load but improves the ride performance and reduces the vehicle masses (SKF, 2011). One of the first popular bogie models was the link suspension bogie, also known as *G bogie*, standardized in Europe by the International Union of Railways (UIC) in the 1950s (Jönsson, 2007). This bogie design has four double link suspensions with leaf springs connecting two wheelsets to a bogie frame on which the rail car is mounted. The evolution of the suspension systems in the second half of the twentieth century led to more sophisticated bogie models which are commonly used in modern trains. Two of most commonly used freight bogies are the *three-piece* and *Y25 bogies*, discussed in the following chapter and considered in this study.

CHAPTER 5

THREE-PIECE AND Y25 BOGIES

In this chapter, the three-piece and the Y25 bogies considered in this investigation are described. The results obtained using the DDS computational approach are used in this investigation to extract performance measures that shed light on the bogie behavior and the effectiveness of the gravity force in balancing the centrifugal force.

5.1 Three-Piece Bogie

The three-piece bogie design, shown in Figure 1, was developed in the United States and is widely used in many other countries. The bogie design has been continuously changed and improved over many decades, leading to different design configurations adopted by several countries, including countries in North and South Americas, Russia, China, India, Australia and African countries.

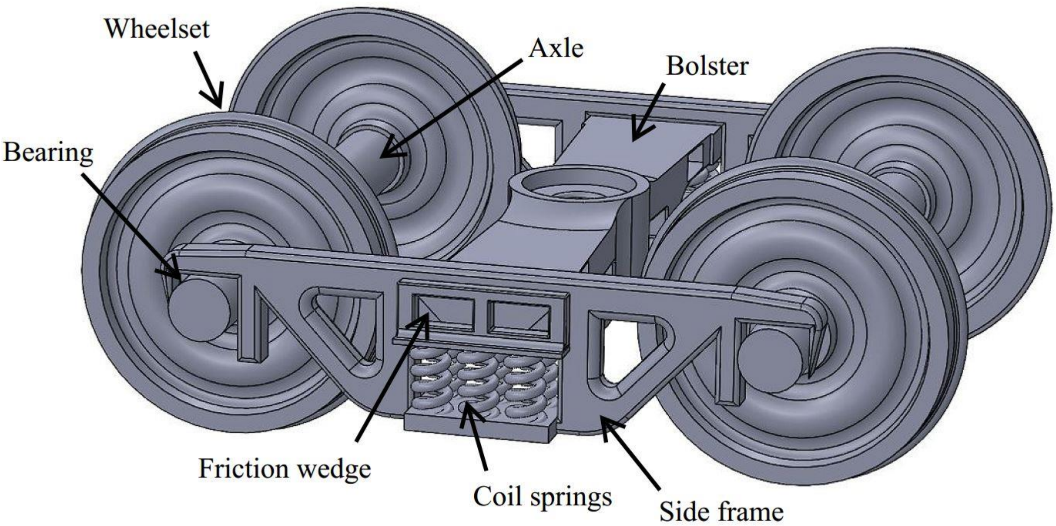

Figure 1: Three-piece bogie

Use of the three-piece bogies is common for heavy vehicles because of its high permissible axle load that reaches 36 tons (Iwnicki, 2015). While these bogies are very durable, their structure is simple and compact, they require a low production and maintenance cost, and their repair and maintenance is simple. However, three-piece bogies have some disadvantages that include higher risk of derailment during curve negotiations and dynamic instability when used with unloaded cars. They also exert higher dynamic loads on the track because of lack of a double suspension system, and this in turn causes increased wear of the wheel and rail surfaces, resulting in higher vibration level and track maintenance cost (Sadeghi et al, 2011).

The three-piece bogie, as its name indicates, consists of three main parts: a bolster and two side frames. The two wheelsets of the bogie are connected to the two side frames by four sets of bearings located at the right and left ends of the axles. The side frames are longitudinal rigid structures on which the bolster is installed horizontally using a suspension system that consists of two sets of coil springs and four friction wedges divided between the two side frames. The coil springs serve to isolate the vibration, and the friction wedges serve as energy-dissipating elements that are alternatives to the hydraulic or pneumatic dampers used in passenger trains. Friction wedges are more common for freight trains because they produce higher friction forces as the axle load increases. A friction wedge, which is a triangular steel block vertically supported by a spring, can be arranged in two different configurations: *constant damping* and *variable damping*. In the constant damping configuration, the spring supporting the wedge is attached to the bolster, while in the variable damping configuration the spring is attached to the lower part of the side frame (Sun and Cole, 2008). The variable damping arrangement, shown in Figure 2, is more common and it is the configuration used in this study. In this configuration, each wedge has a face in contact with a vertical surface of the side frame, while the inclined surface of the wedge is in contact with the bolster. During operation, the friction force resulting from the relative sliding between the contact surfaces leads to energy dissipation proportional to the axle load. The car body is mounted on the *center plate*, centrally placed on the bolster, using a revolute joint that allows for a relative rotation required for improved performance during curve negotiations.

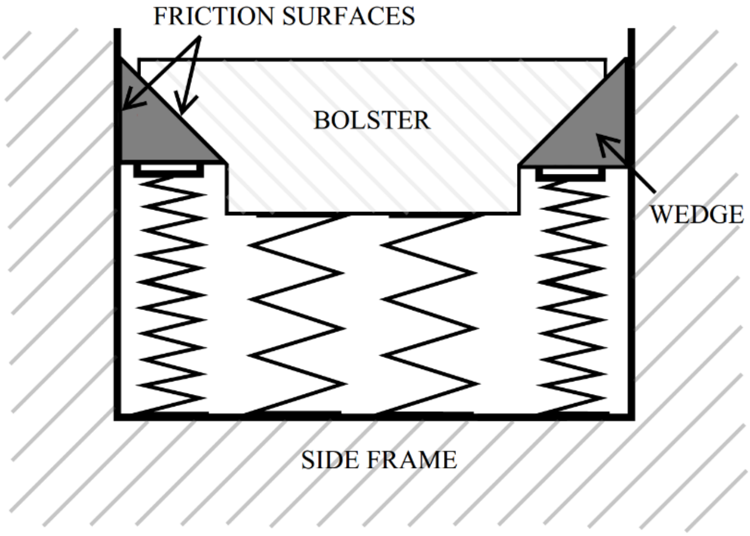

Figure 2: Friction wedge mechanism

5.2 Y25 Bogie

The Y25 bogie, shown in Figure 3, is the second most widely used bogie in modern freight trains. It was developed in France in 1948 and it was standardized in 1967 by the ORE (Office de Recherches et d'Essais) committee (Iwnicki, 2015). The main components of this bogie are two wheelsets, four axle boxes, four spring holders and a frame. As in the three-piece bogie, sets of bearings, placed in axle boxes, are used at the ends of the wheelset axles. The frame is a single rigid structure extended along the whole bogie and it is supported by the primary suspension that consists of four sets of vertical coil springs mounted on the axle boxes. Unlike the three-piece bogie, the suspension is placed closer to each wheel. The damping in the vertical direction is generated by a mechanism called *Lenoir link*, designed to use part of the cargo weight to generate friction that is load-sensitive and proportional to the weight of the car body (Jönsson, 2007).

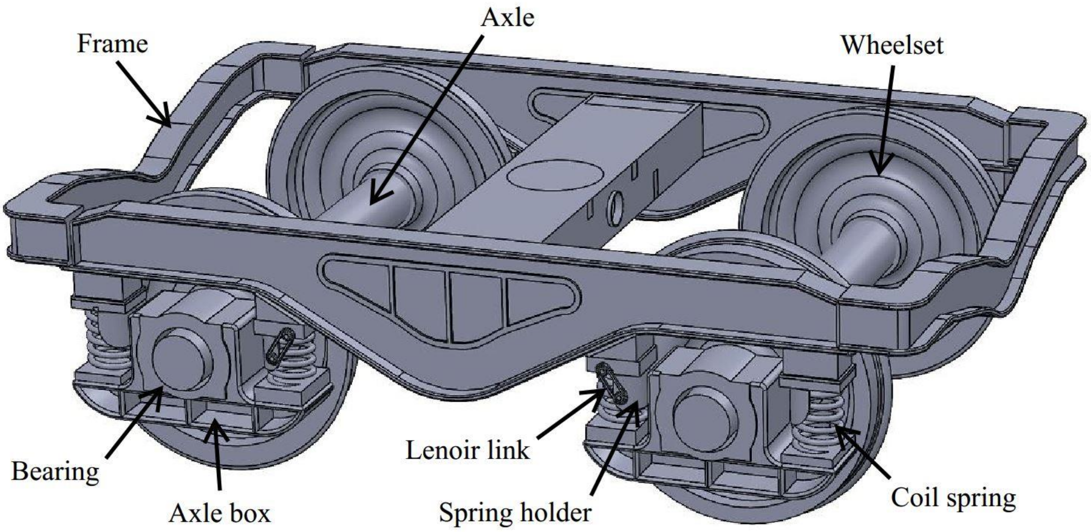

Figure 3: Y25 bogie

A Lenoir link, shown in Figure 4, connects the frame to a spring holder, which is a cap-like device fixed to the tip of one of the springs vertically mounted on the axle box. The spring which supports the spring holder is always the most internal component in the axle box with respect to the center of the bogie, as shown in Figure 3. The Lenoir link is inclined to allow converting the car weight to horizontal and vertical components at the spring holder (Bosso et al, 2002). The vertical component is absorbed by the spring deformation, while the horizontal component is transmitted by the holder to a pusher that is pressed against a vertical surface on the axle box. The vertically oscillating spring holder drags the pusher up and down, generating friction force proportional to the normal force applied by the pusher. This friction mechanism is comparable to the one provided by the friction wedges of the three-piece bogie. The Y25 bogies can also have a secondary suspension consisting of two sets of coil springs located between the frame and the car body. While the admissible Y25 axle loads are not as high as allowed by three-piece bogies, previous studies reported lower risk of derailment during curve negotiations for the Y25 bogie (Kovalev et al, 2009).

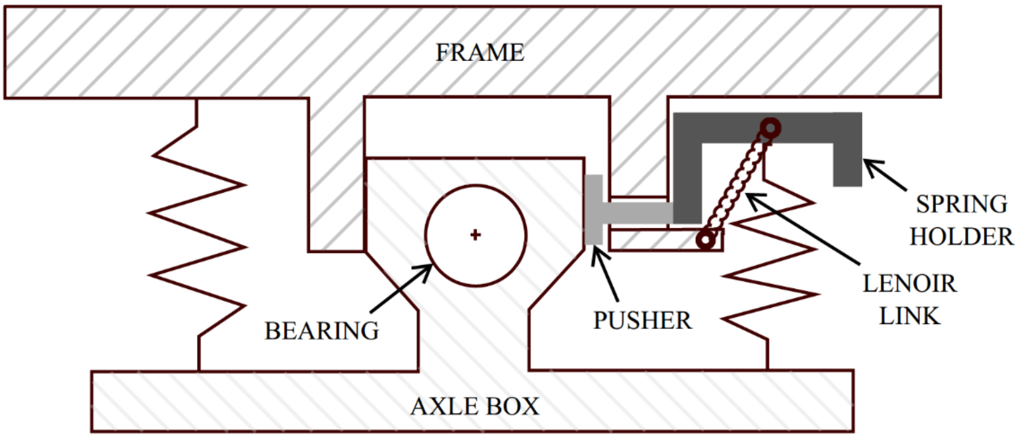

Figure 4: Lenoir link mechanism

CHAPTER 6

GEOMETRY CONSIDERATIONS AND BALANCE SPEED

It was shown that the component of the gravity force that balances the centrifugal force in its totality is given in terms of the Frenet vertical development and bank angles θ and ϕ respectively, by $F_{gn} = mg\cos\theta\sin\phi$. This equation demonstrates that for zero Frenet bank angle ϕ, there is no gravity force component that lies in the motion (osculating) plane regardless of whether or not there is a centrifugal force. The centrifugal force exists when a vehicle traces a curve which may or may not have zero Frenet bank angle. For example, a mass that traces a *helix curve* has a centrifugal force while the Frenet bank angle ϕ of the helix curve is zero (Ling and Shabana, 2021; and Shabana and Ling, 2021). In this case, there is no gravity force component that can be used to balance the centrifugal force. For this reason, the concept of the *Frenet super-elevation* is fundamental for understanding the forces that influence the vehicle motion. The Frenet super-elevation should be distinguished from the track super-elevation, which has proven to be less effective and does not totally prevent wheel-flange/rail contacts, despite its contribution to lower the severity of the impacts.

6.1 Track Super-Elevation

The track super-elevation is used in practice for curved track segments to create a lateral component of the gravity force that balances the lateral component of the centrifugal force. The curved segments of the track are super-elevated by a track bank angle ϕ_t which is different from the Frenet bank angle ϕ. An assumption is made that the vehicle strictly traces a circular curve that lies in a plane parallel to the horizontal plane, and consequently, the centrifugal force in its totality, $m(V)^2/R_t$, is assumed to lie in this plane, where V is the forward velocity of the vehicle along the tangent to the circular curve, and R_t is the radius of curvature of the circular curve. In this case, the lateral component of the centrifugal force is $\left(m(V)^2/R_t\right)\cos\phi_t$ and the lateral component of the gravity force is $mg\sin\phi_t$. By equating these two force components, the balance speed is defined as $V=\sqrt{gR_t\tan\phi_t}=\sqrt{gR_t h/G}$, where h and G are, respectively, the track super-elevation and gage. This definition of the balance speed lacks uniqueness, because the bank angle ϕ_t can be increased and the balance speed V can be increased accordingly. Furthermore, observations of realistic motion scenarios have shown that use of this definition of the balance speed does not prevent wheelsets from moving toward the high and low rails, exerting high impact forces on the rail structure, and maintaining undesirable continuous wheel/rail contact during curving. Therefore, extensive computer simulations performed to obtain recorded motion trajectories offer alternatives for extracting information that will eventually lead to more proper force interpretation.

6.2 Forward Motion and Roller Test Rigs

The forward velocity V along the tangent to the track centerline needs to be distinguished from the velocity $\dot{s}$ along the tangent to the motion trajectory curve. An approximate relationship between the two velocities can be obtained from the definition of the motion trajectory curve velocity vector $\dot{\mathbf{r}}^i=\begin{bmatrix}\dot{x}^i & \dot{y}^i & \dot{z}^i\end{bmatrix}^T$ of component i. If the trajectory coordinates are used, one can write (Shabana, 2021)

$$\dot{\mathbf{r}}^i=\begin{bmatrix}\dot{x}^i & \dot{y}^i & \dot{z}^i\end{bmatrix}^T=\begin{bmatrix}\dot{s}_t^i & \dot{y}_t^i & \dot{z}_t^i\end{bmatrix}^T=\mathbf{r}_s^i\dot{s}^i=\dot{s}^i\begin{bmatrix}r_{s1}^i & r_{s2}^i & r_{s3}^i\end{bmatrix}^T \tag{5}$$

where s_t^i is the arc length of the track centerline, and y_t^i and z_t^i are, respectively, the displacements in the lateral and normal directions with respect to the track centerline. The preceding equation shows that $\dot{s}_t^i = \dot{s}^i r_{s1}^i$. This equation and the definition of the inertia force vector $\mathbf{F}_i^i = m^i \ddot{\mathbf{r}}^i(t) = m^i\left(\ddot{s}\mathbf{r}_s^i + \left((\dot{s})^2/R\right)\mathbf{n}^i\right)$ shed light on the limitation of roller test rigs in which the wheelset forward motion is replaced by rotating rollers that represent the rails. Given the influence of the inertia forces on the dynamics and forces of wheelsets and the wheel/rail contact, the serious limitations of using roller test rigs are obvious. The forward motion has a significant effect on the geometry of the motion trajectory curves and on the definitions of the unit tangent and normal vectors $\mathbf{r}_s^i$ and $\mathbf{n}^i$, respectively.

6.3 Frenet Force Balance and Recorded Motion Trajectories

Recorded motion trajectories can be accurately measured using vehicles instrumented with advanced sensors, or can be obtained using computer simulations of detailed virtual models. To have proper force interpretation, it is important to distinguish between the geometry of the track and the geometry of the motion trajectory. This distinction can be made by distinguishing between the track curvature, vertical development, and bank angles, denoted respectively as ψ_t, θ_t, and ϕ_t, and the motion trajectory Frenet curvature, vertical development, and bank angles ψ, θ, and ϕ, respectively. For example, on a tangent track, the track curvature, vertical development, and bank angles can all be zero, that is, $\psi_t = 0, \theta_t = 0$, and $\phi_t = 0$, while the Frenet angles are different from zero because of the hunting oscillations which define motion trajectory curves with Frenet curvature, vertical development, and bank angles that can be different from zero.

The recorded motion trajectory curves can be used to provide precise definition of the *balance speed*; this is with the understanding that motion trajectories are not a priori known. Nonetheless, more precise definition of the balance speed based on extensive computer simulations can create the knowledge and provide force interpretations that allow for developing more credible operation and safety guidelines. The definition of the balance speed based on the fixed-in-time track geometry and given by $V = \sqrt{gR_t \tan\phi_t} = \sqrt{gR_t h / G}$ is derived using a strict assumption that cannot be fulfilled in realistic motion scenarios and does not account for the actual motion and forces acting on the system. To develop a more precise definition based on the assumption that $V = \dot{s}_t^i = \dot{s}^i r_{s1}^i$ is the operating vehicle velocity, an osculating plane force balance can be used. It is clear from the equation $V = \dot{s}^i r_{s1}^i$ that in the case of a forward motion with non-zero V, $\dot{s}^i r_{s1}^i \neq 0$. The osculating plane component of the gravity force is $F_{gn} = mg\cos\theta\sin\phi$ and the centrifugal force, which is in the direction of the normal vector that lies in the osculating plane, is defined as $m\left(\dot{s}^i\right)^2 / R = m\left(V / r_{s1}^i\right)^2 / R$. Equating these two osculating plane force components, a precise definition of the balance speed can be obtained as

$$V = r_{s1}^i \sqrt{Rg\cos\theta\sin\phi} \tag{6}$$

Because R is the radius of curvature, the definition of the balance speed given by the preceding equation is function of all the three Frenet angles which are motion dependent. The only constant in this definition is the gravity constant g. It is also important to point out a fundamental difference between the balance speed in the preceding equation and the balance speed definition based on the motion-independent track geometry. The definition of the balance speed in the preceding equation assumes that the osculating plane component of the gravity force balances the centrifugal force in its totality. In the definition used in practice, on the other hand, the lateral component of the gravity force is assumed to balance only the lateral component of the centrifugal force.

6.4 Angle of Attack

A geometric measure for the bogie curving behavior is the *angle of attack* of a wheelset, defined as the angle between the forward velocity vector of the wheelset and the longitudinal tangent to the rail at the contact point. That is, the angle of attack α is defined as $\alpha = \cos^{-1}\left(\mathbf{V}^w \cdot \mathbf{t}^r / \left|\mathbf{V}^w\right|\left|\mathbf{t}^r\right|\right)$, where $\mathbf{V}^w$ is the wheel velocity vector and $\mathbf{t}^r$ is the longitudinal rail tangent at the wheel/rail contact point. The angle of attack defines orientation of the wheelset with respect to the rail as shown in Figure 5.

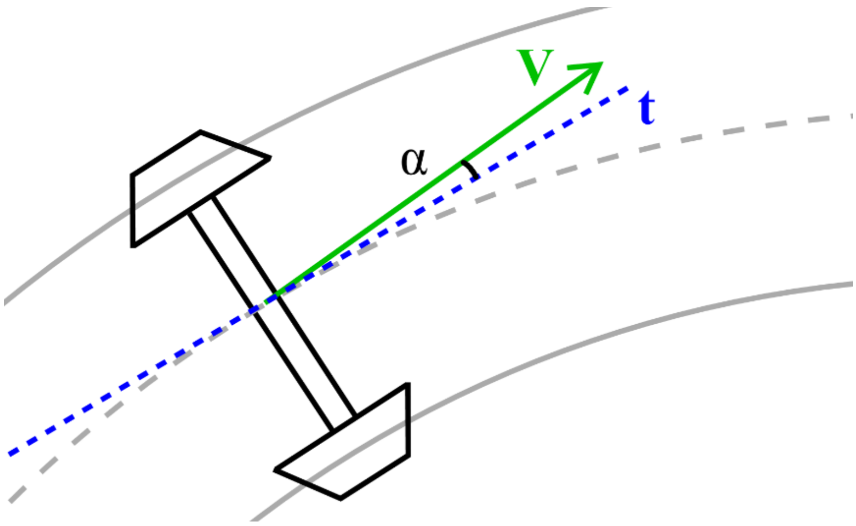

Figure 5: Angle of attack

A smaller angle of attack is an indication that the wheelset is following the track curve, while a larger angle of attack indicates a larger deviation from the desired trajectory and the possibility of wheel climb. Previous investigations have shown that the angle of attack is related to and influenced by the wheel/rail contact forces and slippage and has an effect on the wear of the rail and wheel flange surfaces (He and McPhee, 2005). Value of the angle of attack is related to the distance required for a complete wheel climb; the larger the angle of attack is, the higher the risk of derailment due to wheel climb (Kataori et al, 2011). Previous studies have shown that the angle of attack of a wheelset travelling on a track with variable radius of curvature generally ranges from 0 to 0.5° (Dumitriu, 2012; He and McPhee, 2005; Kataori et al, 2011).

CHAPTER 7

CONCEPT DEMONSTRATION

In this chapter, a simple example is used to demonstrate the concepts discussed in this investigation before presenting the three-piece and Y25 bogies results in the following chapter. For this purpose, a single unsuspended wheelset model travelling freely on a curved track with a forward velocity of 15 m/s is used. The wheelset is subjected to an initial lateral velocity of 0.3 m/s to initiate the hunting oscillations. The track used in this example is the same as the one described in Chapter 8. The wheelset mass is assumed 1568 kg and the mass moments of inertia are $I_{xx} = I_{zz} = 656$ kg.m^2 and $I_{yy} = 168$ kg.m^2. The wheelset is considered rigid and equipped with the APTA 120 wheels described in more detail in Chapter 8.

Figure 6 shows the track bank angle ϕ_t for various track sections that include tangent, spiral, and curve sections. The results presented in this figure show that the track bank angle is zero for the tangent sections and non-zero for the spiral and curve sections. The magnitude of the wheelset centrifugal force is shown in Figure 7 for two cases. The first is the magnitude of the centrifugal force computed using the track geometry and defined as $m\left(V\right)^2 / R_t$, while the second is the magnitude of the centrifugal force obtained using the recorded motion trajectories and is defined as $m\left(\dot{s}\right)^2 / R$. Superscript i is removed for simplicity of the figure caption notation.

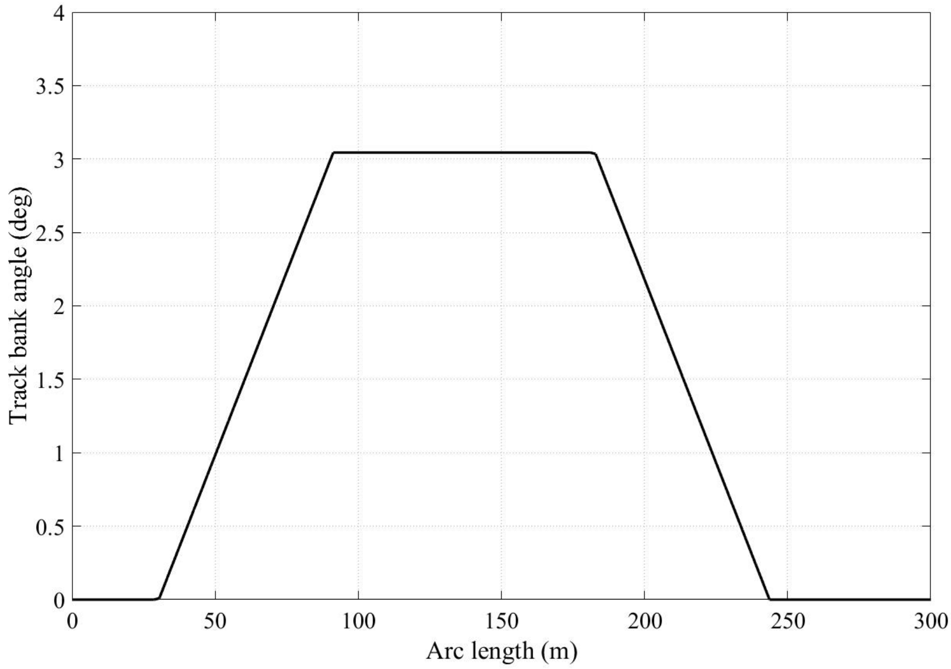

Figure 6: Track bank angle

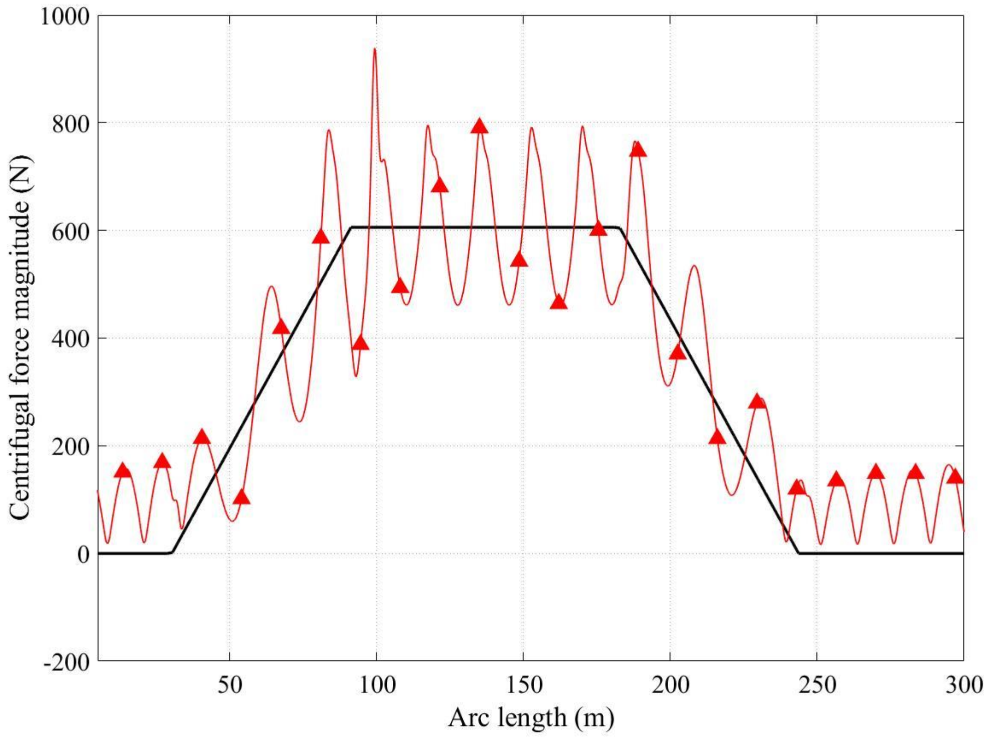

Figure 7: Centrifugal force for the unsuspended wheelset (—— $m(V)^2/R_t$,

—▲— $m(\dot{s})^2/R$)

It is clear from the results presented in Figure 7 that there is a significant difference between the magnitudes of the two forces, and such a difference cannot be ignored even in the case of a simple wheelset with a mass much smaller than the laden freight cars. Furthermore, the magnitude of the centrifugal force computed using the motion trajectories is oscillatory reflecting the nature of the hunting oscillation of the wheelset. These oscillations are not captured by the definition of the centrifugal force used in practice based on the motion-independent track geometry. Moreover, as previously discussed, the centrifugal force can be significantly different from zero when negotiating the tangent sections of the track as demonstrated by the results presented in Figure 7. To verify the tangent section results presented in Figure 7, the centrifugal force along the tangent segments is computed using the equation $|\mathbf{F}_{ice}| = m(\omega_h)^2 Y_h \sin(\omega_h t + \beta)$, derived from Klingel's geometrical analysis, where m is the wheelset mass, t is time, ω_h and Y_h are, respectively, the frequency and amplitude of the hunting oscillations, and β is a phase angle (Shabana, 2021). The tangent track centrifugal force results obtained using this simple equation based on pure geometric analysis show a remarkable agreement with the results obtained using the fully nonlinear MBS simulation of the wheelset. The results of the track bank angle shown in Figure 6 are consistent with the prediction of the centrifugal force as defined by the track geometry.

To analyze the direction of the centrifugal force vector, which is parallel to the unit vector normal to the curve, the Frenet bank angle obtained using the motion trajectory curve is plotted in Figure 8 and it can be compared with the track bank angle. Zoomed plots are used to demonstrate the differences since bank angles are normally small and their amplitude can be small in comparison with the values due to the discontinuities at the track transitions, marked by the vertical dashed lines.

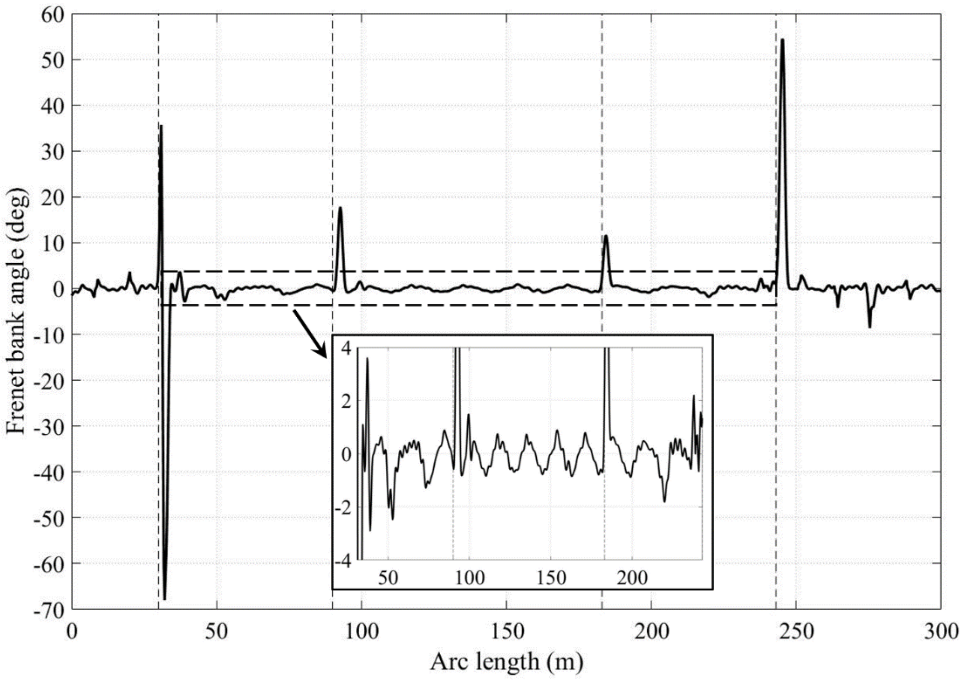

Figure 8: Unsuspended wheelset Frenet bank angle

The results of the track and Frenet bank angles presented in Figure 8 show differences attributed to the fundamental difference in the definition of these two angles; one is motion-independent, while the other is motion-dependent. Furthermore, the Frenet bank angle is sensitive to the discontinuities at the track section transitions at which higher degrees of continuity are not enforced. The track bank angle obtained by linear interpolation does not exhibit this sensitivity. An important and interesting observation from the results shown in Figure 8 is the large Frenet bank angle when the wheelset negotiates the tangent sections of the track due to the hunting oscillations. By examining the zoomed plot, it is possible to see that the Frenet bank angle varies between -1° and 1° and it has oscillations similar to the centrifugal force oscillations. Figure 9 shows comparison between components of the gravity force in the track plane and the osculating plane. The former is defined by the equation $mg\sin\phi_t$, while the latter is defined by the equation mgn_3, where n_3 is the third element of the unit vector normal to the motion trajectory curve.

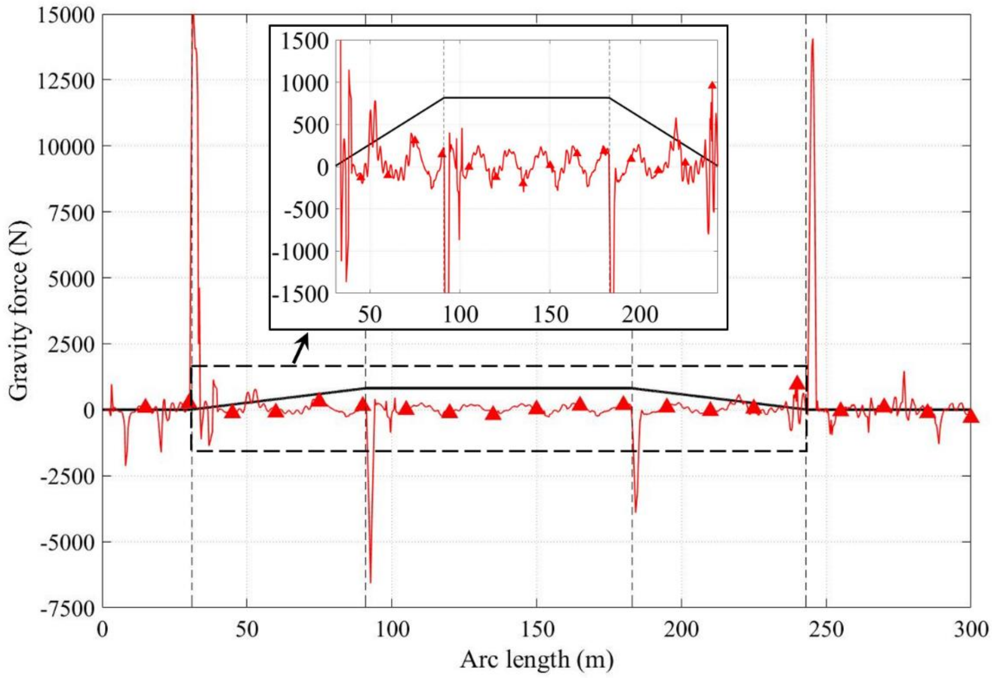

Figure 9: Gravity force component in the track and the osculating plane (—— Track plane, —▲— Osculating plane)

CHAPTER 8

BOGIE/TRACK SIMULATION MODELS

In this chapter, computer simulation models of the three-piece and Y25 bogies, track and friction contact are described. The computer models are analyzed using a nonlinear MBS algorithm based on a three-dimensional wheel/rail contact formulation. Each bogie model consists of several rigid bodies interconnected by joints and force elements. The bogie models are assumed to travel on a track with tangent, spiral, and curve sections. Because the inertia, material, and geometric properties used in this investigation are not exact, the kinematic and force results will be presented in the following chapter without making judgements on the overall bogie performance, as previously mentioned. Therefore, the results presented in the following chapter serve to explain new concepts used in the *Frenet force balance*. The motion trajectories will be obtained using the software **SIGMA/SAMS** (**S**ystematic **I**ntegration of **G**eometric **M**odeling and **A**nalysis for the **S**imulation of **A**rticulated **M**echanical **S**ystems).

8.1 Three-Piece Bogie Model

The three-piece bogie model used in this investigation is based on the model presented by Sun and Cole (2008). This bogie model, despite its simplicity, can exhibit simulation instabilities due to the nonlinear characteristics of its friction elements. The bogie model is assumed to consist of nine bodies: two wheelsets, two side frames, four friction wedges and a bolster. The distance between front and rear wheelsets is 2.591 m and the bolster center of mass has initial vertical position of 0.457 m. The inertia properties used in the simulations are listed in Table 1.

TABLE 1: INERTIA PARAMETERS FOR THE THREE-PIECE BOGIE MODEL

Wheelsets	**Side Frames**	**Bolster**	**Friction Wedges**
$m = 1500$ kg $I_{xx} = 420$ kg.m^2 $I_{yy} = 100$ kg.m^2 $I_{zz} = 420$ kg.m^2	$m = 469$ kg $I_{xx} = 100$ kg.m^2 $I_{yy} = 115$ kg.m^2 $I_{zz} = 115$ kg.m^2	$m = 500$ kg $I_{xx} = 175$ kg.m^2 $I_{yy} = 10$ kg.m^2 $I_{zz} = 175$ kg.m^2	$m = 10$ kg $I_{xx} = 0$ kg.m^2 $I_{yy} = 0$ kg.m^2 $I_{zz} = 0$ kg.m^2

The leading wheelset of the bogie is assumed to travel with a prescribed constant forward velocity of 17.4 m/s along the track centerline. The side frames are attached to the ends of the wheelsets axles by bearing elements which generate forces proportional to the relative displacement and velocity between the two bodies connected by the bearing elements. The bearing stiffness and damping coefficients are assumed 1.75×10^7 N/m and 1.75×10^5 N.s/m, respectively. Side frames are connected to the bolster by springs modeled using bushing elements. In the computer model, two vertical-axis springs are used to connect each side frame to the bolster. The springs have a vertical stiffness coefficient 1.69×10^6 N/m, vertical preload 4×10^4 N, and lateral and longitudinal stiffness coefficients 1×10^6 N/m. In this arrangement, the lateral and longitudinal stiffness is approximately 60% of the stiffness in the vertical direction. The same vertical stiffness and preload are used for the springs that support the friction wedges, each is assumed to have mass of 10 kg and negligible mass moments of inertia. The bolster, placed transversally with respect to the side frames, is modeled as a rigid beam whose ends are located just above the wedges. Each wedge has a vertical friction surface in contact with the side frame and a 45° inclined friction surface in contact with the bolster. The friction surface formulation is explained in more detail in Sub-chapter 8.5. The bolster has the freedom to move vertically with respect to the side frames, but the relative yaw rotation and longitudinal displacement are restricted by using two vertical-axis cylindrical joints between the side frames and the ends of the bolster.

8.2 Y25 Bogie Model

The Y25 bogie model used in this study is based on the model proposed by Bosso et al (2002). The bogie components considered are two wheelsets, four axle boxes, four spring holders and a frame. The distance between the front and rear wheelsets is assumed 2.591 m and the center of mass of the frame has the same initial vertical position of 0.457 m. The inertia properties used in the computer simulations are provided in Table 2.

TABLE 2: INERTIA PARAMETERS FOR THE Y25 BOGIE MODEL

Wheelsets	**Axle Boxes**	**Spring Holders**	**Frame**
$m = 1225$ kg $I_{xx} = 750$ kg.m^2 $I_{yy} = 140$ kg.m^2 $I_{zz} = 750$ kg.m^2	$m = 50$ kg $I_{xx} = 0$ kg.m^2 $I_{yy} = 0$ kg.m^2 $I_{zz} = 0$ kg.m^2	$m = 5$ kg $I_{xx} = 0$ kg.m^2 $I_{yy} = 0$ kg.m^2 $I_{zz} = 0$ kg.m^2	$m = 2500$ kg $I_{xx} = 1400$ kg.m^2 $I_{yy} = 2000$ kg.m^2 $I_{zz} = 2500$ kg.m^2

The front wheelset has a prescribed forward velocity of 17.4 m/s. The axle boxes are connected to the ends of the wheelset axles using bearing elements. For the first suspension, two vertical springs are attached to each wheelset: one supports the frame and the other supports a spring holder. These springs are modeled using bushing elements with the same parameters as those used for the three-piece bogie model. The Lenoir links connecting the four spring holders to the frame are modeled as bushing elements, but with a relatively high stiffness, equal to 2×10^7 N/m, to ensure negligible link deformation and direct force transmission from the frame to the spring holder. Because Lenoir links are inclined of 60° with respect to the horizontal plane, the transmitted force has vertical and horizontal components. The friction is considered using vertical friction contact surfaces between each spring holder and axle box. During the motion, the bushing element representing the Lenoir link pushes the spring holder against the axle box and friction forces are generated.

8.3 Track Model

The 300 m track model used has 1.435 m gage and starts with 30 m tangent segment, followed by 60 m spiral for transition to a left 90 m - 3 degree curve with radius of curvature 582 m, followed by a 60 m spiral segment connected to a final 60 m tangent segment. Considering a constant vehicle speed of 17.4 m/s, the total travel time is approximately 18 s. Figure 10 shows the track geometry defined by its lateral and vertical coordinates.

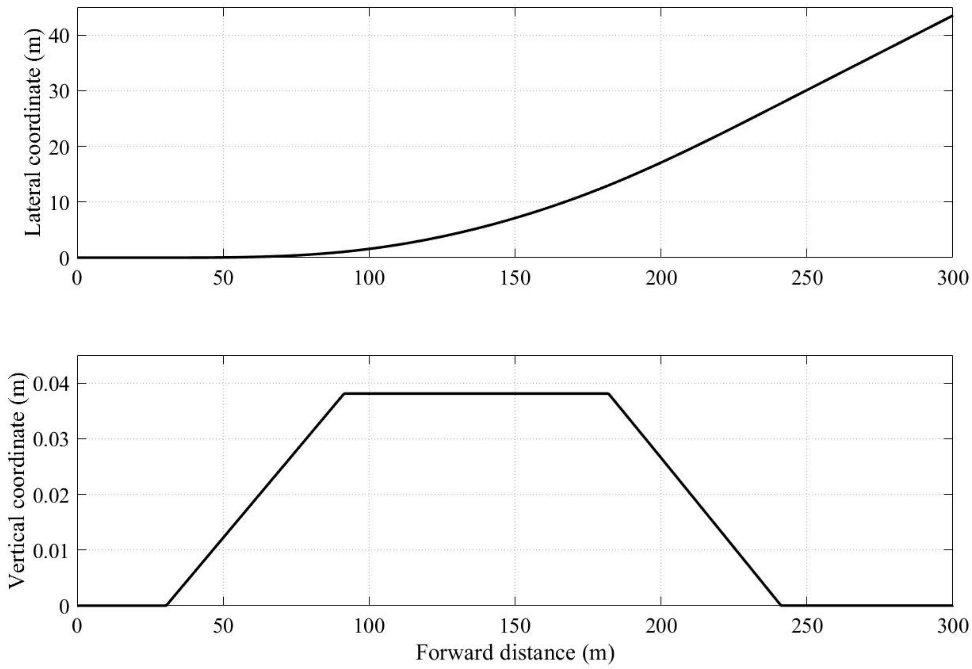

Figure 10: Track geometry

The rail profile used in the three-piece bogie simulation is the standard 140 lb wheel profile given by AREMA (American Railway Engineering and Maintenance-of-Way Association). For the Y25 bogie simulation, a standard UIC54 rail, manufactured according to European Standard EN 13674-1, is adopted.

In developing the track model, a preprocessor computer program is used to determine a track point mesh geometry data file based on the standard industry inputs: horizontal curvature, grade, and super-elevation. These standard industry inputs at points at which the track geometry changes are used to define position coordinates and orientation angles at nodal points. The position and angle coordinates are used with an interpolation based on the *absolute nodal coordinate formulation* (ANCF) to define the track geometry at arbitrary points within the segments defined by the track nodes. This ANCF representation ensures gradient continuity at the nodes but does not ensure curvature continuity at the track transitions. Because of this numerical representation, spikes can be observed in the numerical results due to the curvature discontinuities at the intersections of track segments with different curvature values.

8.4 Wheel Profiles

The wheelsets have axles with diameter 0.1 m and length of 2.06 m. Freight trains standard wheel diameters range from 840 to 920 mm, while the standard width is approximately 130 mm (RailCorp Engineering Standard, 2013). The wheel diameter and width used in the simulations are, respectively, 914 mm and 135 mm. Two different wheel profiles are used for the two bogies: an American standard for the three-piece bogie and a European one for the Y25 bogie. For the three-piece bogie, the APTA 120 profile is chosen. This profile, provided by the American Public Transportation Association (APTA), is based on an older AAR S-621-79 profile previously proposed by the Association of American Railroads (AAR). The APTA 120 profile has conicity of 1:20 (5% slope), flange angle 72° and flange height 1 inch (The American Public Transportation Association, 2007). For the Y25 bogie, the P1 profile extracted from the Railway Group Standard GMRT2466 is chosen. This profile, based on BR (British Rail) drawing S8 C2-8006234, has tread slope of 5%, flange angle 60° and flange height 29.93 mm (Rail Safety and Standards Board, 2017). The two wheel profiles are shown in Figures 11 and 12.

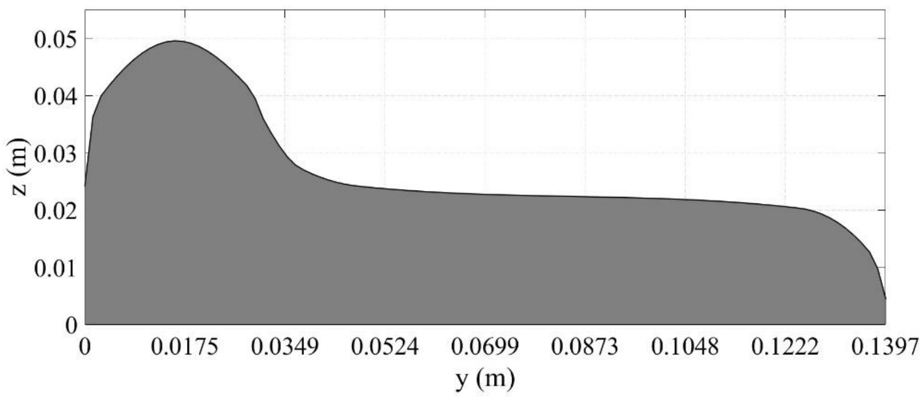

Figure 11: APTA 120 wheel profile

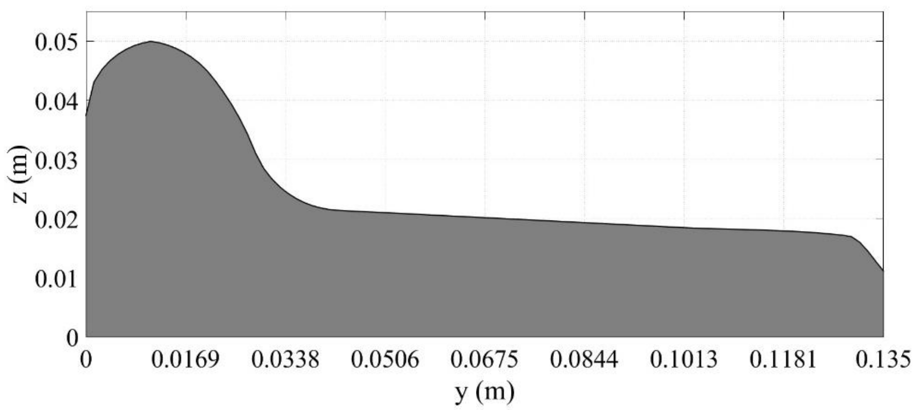

Figure 12: P1 wheel profile

The friction coefficient between the wheels and rails is assumed 0.5 and the wheel and rail materials are assumed steel with modulus of elasticity 210 GPa and shear modulus 82 GPa.

8.5 Friction Elements

Friction damping forces are challenging to model and can be source of numerical instability. In the three-piece bogie, there are eight friction contacts: four on the inclined surfaces between the bolster and wedges and the other four on the vertical surfaces between wedges and side frames. In the case of the Y25 bogie, on the other hand, there are four friction contacts between the spring holders and the axle boxes. A compliant force model is used in this study to model all friction contacts. In this compliant force model, the force component normal to the contact surfaces is assumed to have an elastic force term proportional to the surface penetration δ and a damping force term proportional to the penetration rate. The penetration between two bogie components i and j, projected along the direction of the outward normal to the contact surfaces $\bar{\mathbf{n}}^j$, defined in body j coordinate system, can be written as $\delta = (\mathbf{R}^i + \mathbf{A}^i\bar{\mathbf{u}}^i - \mathbf{R}^j - \mathbf{A}^j\bar{\mathbf{u}}^j)\cdot\left(\mathbf{A}^j\bar{\mathbf{n}}^j\right)$, where $\mathbf{R}^i$ and $\mathbf{R}^j$ are the global positions of the centers of mass of the two components, $\bar{\mathbf{u}}^i$ and $\bar{\mathbf{u}}^j$ are the local position vectors of the two contact points with respect to their component center of mass, and $\mathbf{A}^i$ and $\mathbf{A}^j$ are the rotation matrices that define the orientations of the component coordinate systems. The vector of relative velocity at the contact point can be written as $\mathbf{v}_r^{ij} = \dot{\mathbf{R}}^i + \boldsymbol{\omega}^i \times \left(\mathbf{A}^i\bar{\mathbf{u}}^i\right) - \dot{\mathbf{R}}^j - \boldsymbol{\omega}^j \times \left(\mathbf{A}^j\bar{\mathbf{u}}^j\right)$, where $\boldsymbol{\omega}^i$ and $\boldsymbol{\omega}^j$ are the absolute angular velocity vectors of the two bodies. Using the penetration and the vector of relative velocity, the normal component of the contact force can be defined as $f_n = k\delta + c_n\left(\mathbf{v}_r^{ij}\cdot\mathbf{n}^j\right)$, where $\mathbf{n}^j = \mathbf{A}^j\bar{\mathbf{n}}^j$, and k and c_n are assumed stiffness and damping coefficients. In the numerical study performed in this investigation, the stiffness and damping coefficients are assumed $k = 1\times10^6$ N/m and $c_n = 1\times10^3$ Ns/m, respectively. Using the normal force, the tangential friction force can be computed using the coefficient of dry friction μ as $f_t = \mu f_n$. In this study, the coefficient of dry friction μ is assumed 0.5. This tangential force acts in a direction opposite to the one of the relative velocity between the two contact surfaces.

8.6 Modeling Assumptions

In the bogie models involved in this study, the car body weight is not considered to focus the attention on the bogie performance. Because the axle loads for these bogies are different, more investigations are needed in the future to have better understanding of the bogie behavior when used to support laden rail cars. Because actual bogie designs may include more springs in the suspension, the reduced number of springs used in the models considered in this investigation represent equivalent spring systems. Furthermore, the stiffness coefficients of the springs are assumed constant for simplicity despite the fact that the actual springs can have nonlinear characteristics which are not available to the authors. Use of linear spring models can be justified in the case of small spring deflections. According to the BS EN 16235:2013 standard, the suggested stiffness of vertical tare springs is around 1.2×10^6 N/m for the Y25 bogie. However, a stiffness of 1.69×10^6 N/m is adopted to be consistent with the spring coefficient used for the three-piece bogie, to have a more meaningful comparison between the two designs.

In the Y25 bogie design, the longitudinal motion of axle boxes is restricted to a stroke of few millimeters by limiting the yaw oscillations of the wheelsets. Such a restriction is not considered in this investigation, since axle box displacements are small because the curve used is not very tight.

CHAPTER 9

NUMERICAL RESULTS

Numerical results of the MBS dynamic simulations of the three-piece and Y25 bogies are presented in this chapter. The results are obtained by considering only the individual bogies without the rail car in order to have clear understanding of the bogie behavior without considering other loading conditions that can influence the motion characteristics. More future and focused investigations are needed to understand the effect of heavier axle loads on the bogie performance. Because of the large number of design variants of each bogie type and the difficulties of obtaining exact inertia, dimension, and suspension data, the results are presented in this chapter without making an overall judgement on the bogie performance.

9.1 Angle of Attack

The angle of attack is computed and plotted for the front and the rear wheelsets of each bogie, as shown in Figures 13 and 14. Figure 13 presents the results that compare the angle of attack for the front wheelset, while Figure 14 shows the comparison for the rear wheelset. The results presented in these two figures show, as expected, that the leading wheelset has more variations in the angle of attack as compared to the rear wheelset. Also, as expected, spikes in the angle of attack are observed at the points of transition between different track segments. The non-zero values of the angle of attack shown in these figures do not always imply wheel-flange/rail contact. The results show that the angle of attack oscillates around zero along the tangent segments while it assumes a rather constant nonzero value along the curve, indicating a wheel-flange/rail contact during the curve negotiation. The motion on the first and second spiral segments is characterized by a near linear variation of the angle of attack. This implies, as expected, that deviation of the wheelset from the track orientation starts increasing at the beginning of the spiral segments and reaches a stable value during the curve, a trend confirmed by results presented in previous investigations (He and McPhee, 2005).

By comparing the results of the two bogies, it can be seen that the angle of attack of the Y25 bogie front wheelset has larger perturbations at the track transitions as compared to the three-piece bogie, particularly at the intersection between the curve and the second spiral segment. However, at the same point, a large spike in the angle of attack of the rear wheelset of the three-piece bogie can also be observed. The largest value of the angle of attack observed in the simulations was found to be 1.4°. Based on the results obtained in this study, the leading wheelset seems to have smaller angle of attack in the three-piece bogie, while the rear wheelset of the Y25 bogie has a smaller angle of attack.

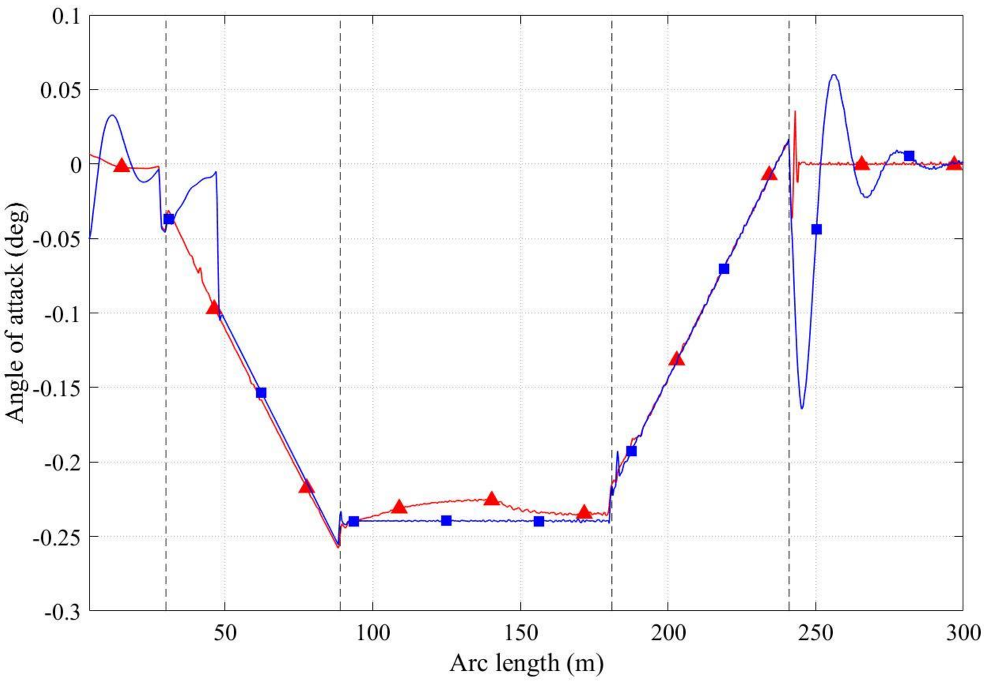

Figure 13: Angle of attack of the leading wheelset (—▲— Three-piece bogie, —■— Y25 bogie)

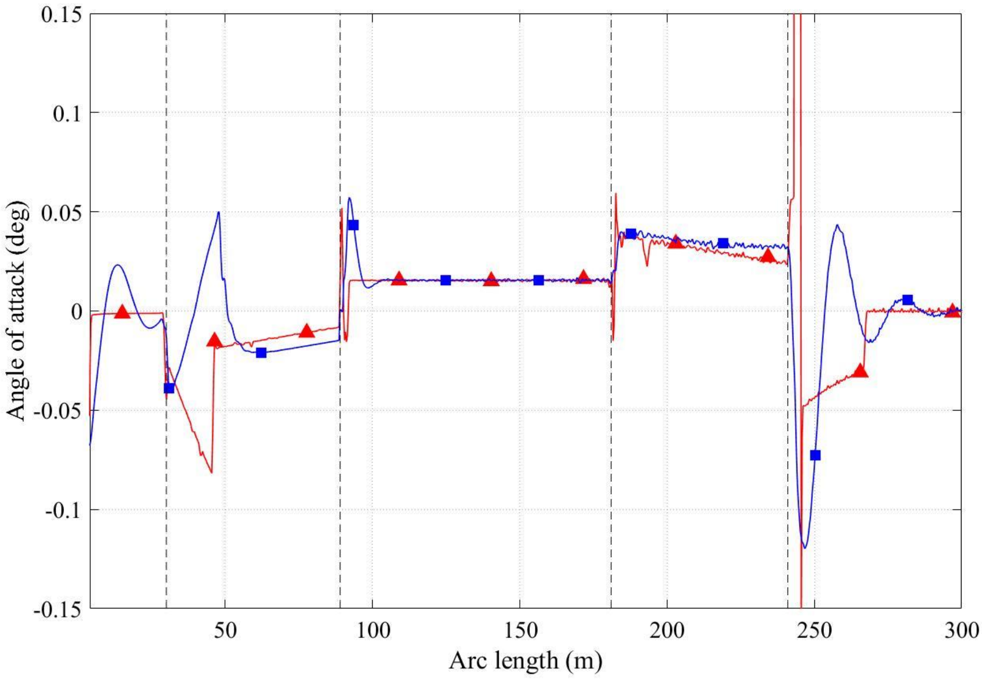

Figure 14: Angle of attack of the rear wheelset (Three-piece bogie, Y25 bogie)

9.2 Flange Contact Forces

Figures 15 and 16 show the flange contact forces that arise during simulations of the three-piece and Y25 bogies. The results presented in these figures can be used to explain the problems associated with the lateral force balance currently used in practice to determine the balance speed. It can be observed from the results presented in Figures 15 and 16 that the front wheelset of the three-piece bogie has a flange contact only during the second spiral segment, while the left rear wheelset flange maintains contact with large section of the first spiral segment and along the entire curve. A similar behavior is observed for the front wheelset of the Y25 bogie, which is the only wheelset that experiences flange contact for this bogie model.

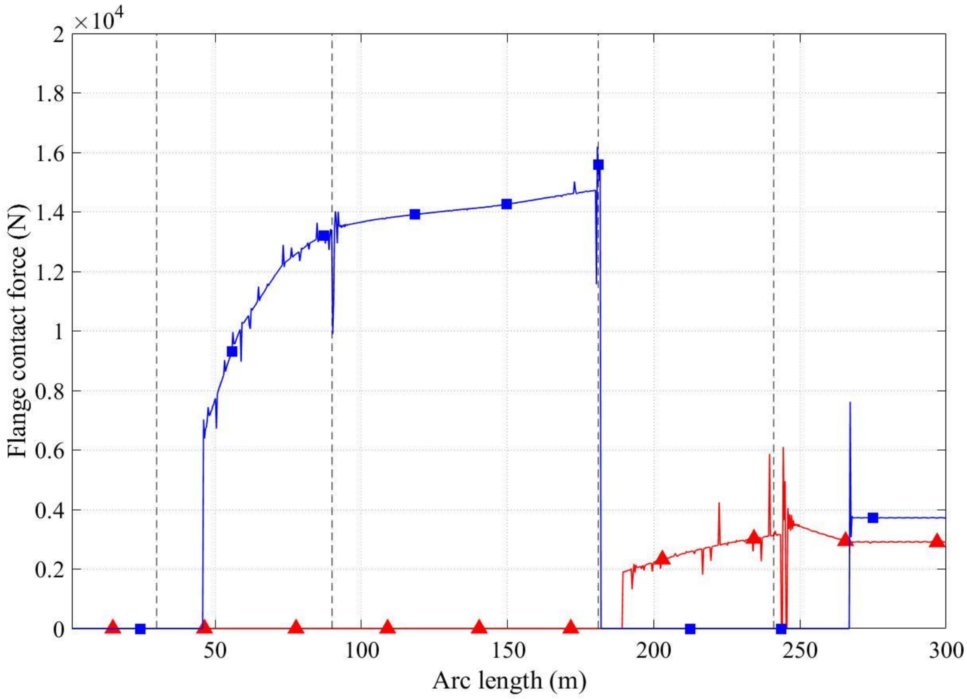

Figure 15: Flange contact forces of the three-piece bogie (Front right contact, Left rear contact)

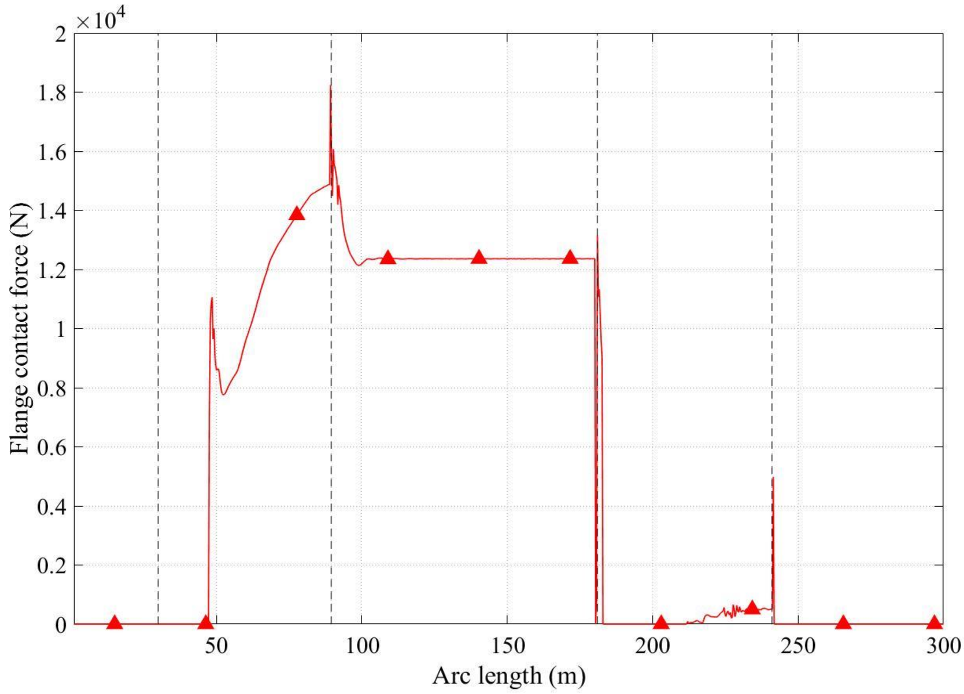

Figure 16: Flange contact forces of the Y25 bogie (Front right contact)

Because simulations are performed at the balance speed, if the equilibrium condition between the lateral component of the centrifugal inertia and gravity forces was achieved, wheel/rail contacts could be avoided during the curve negotiation. In view of these results, the performance of the leading wheelset of the three-piece bogie is better compared to the Y25 bogie. However, the rear wheelset of the Y25 bogie appears to smoothly follow the track, a behavior which is not observed for the three-piece bogie.

9.3 Centrifugal Force

The centrifugal forces of the bogie components can be evaluated considering motion trajectories predicted using the MBS simulations as previously discussed in this paper. To have a more useful representation of the centrifugal force for the multi-component bogies, one can compute the vector sum of all the centrifugal forces of the components based on their actual motion trajectories predicted using the DDS approach described in this paper. Using this approach, the total sum of the centrifugal forces can be determined, but the resultant vector is not associated with a particular point of application on a particular bogie component. Furthermore, the distances between the mass centers of individual components lead to moments that are not considered using this approach. For these reasons, the result of the force sum adopted in this paper serves as an index of the centrifugal force magnitude rather than an actual centrifugal force measure. The simulation-based motion trajectory results are compared with the results obtained from the lateral track plane force equilibrium used in practice to determine the balance speed based on the track geometry instead of the recorded motion trajectories. Figures 17 and 18 show the difference between the two methods used for computing the centrifugal forces.

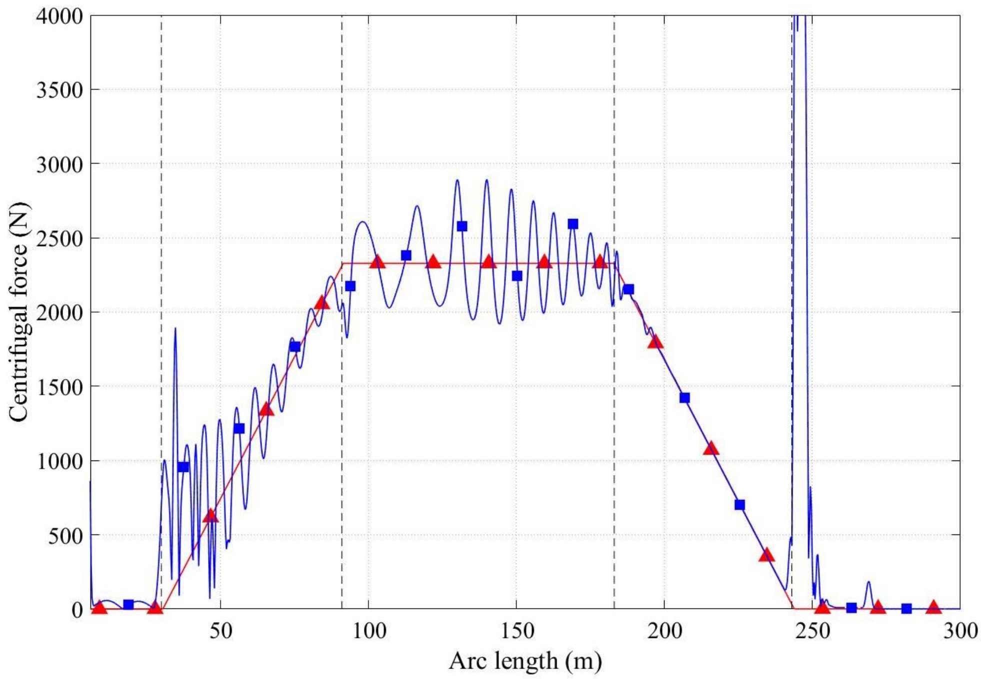

Figure 17: Centrifugal force magnitude of the three-piece bogie (—▲— Track geometry, —■— Motion trajectories)

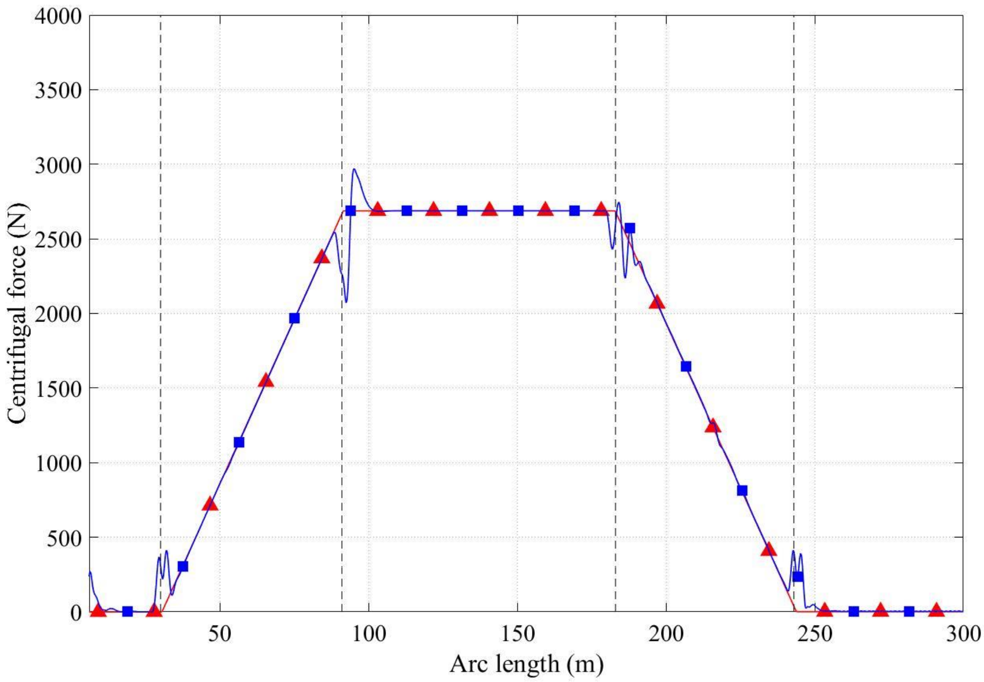

Figure 18: Centrifugal force magnitude of the Y25 bogie (—▲— Track geometry, —■— Motion trajectories)

In case of the three-piece bogie, magnitude of centrifugal force appears to be more oscillatory and the force spike at the end of the second spiral reaches 7700 N. On the other hand, the magnitude of the centrifugal force of the Y25 bogie follows the expected trend, with small perturbations only at the track transitions. Therefore, the trajectory traced by the Y25 bogie is more likely to have less deviations from the track centerline.

9.4 Frenet Bank Angle

Figures 19 - 22 show the Frenet bank angle computed for the wheelsets of the three-piece and Y25 bogies using the recorded motion trajectories. These results can be compared with the motion-independent track bank angle used in practice. The Frenet bank angle defines the super-elevation of the motion plane, while the track bank angle defines the super-elevation of the track plane. Since the centrifugal force acts in the direction of the curve normal vector, which lies in the motion plane, a non-zero Frenet bank angle indicates violation of assumption of horizontal centrifugal force used in practice to define the balance speed.

Along the tangent segments, even if the lateral and vertical deviations of the motion trajectory from the track centerline are small, the Frenet bank angle appears to be sensitive to the change of the curvature of the motion trajectory curves which can represent very tight curves. Near the start of the first spiral and end of the second spiral, spikes due to the track transitions can be observed for all wheelsets, particularly the rear ones. When the Frenet bank angle is zero, the centrifugal force lies in a plane parallel to the horizontal plane, which is the assumption currently made in defining the balance speed. It is important to notice, from the results presented in Figures 19 - 22, that this condition is only met in case of flange contacts, a situation which is not desirable because of the forces exerted on the vehicle and the track structure that can lead to significant wear or possibly derailments. The wheel-flange/rail contact is a clear indication that the track plane lateral force equilibrium used in practice to define the balance speed is violated and does not prevent the vehicle from sliding toward the high or low rail. The results presented in Figures 19 - 22 show that the Frenet bank angle has more oscillations for the three-piece bogie front wheelset and for the Y25 bogie rear wheelset. Larger Frenet bank angle can imply higher level of force self-balancing by the component of the gravity force in the osculating plane.

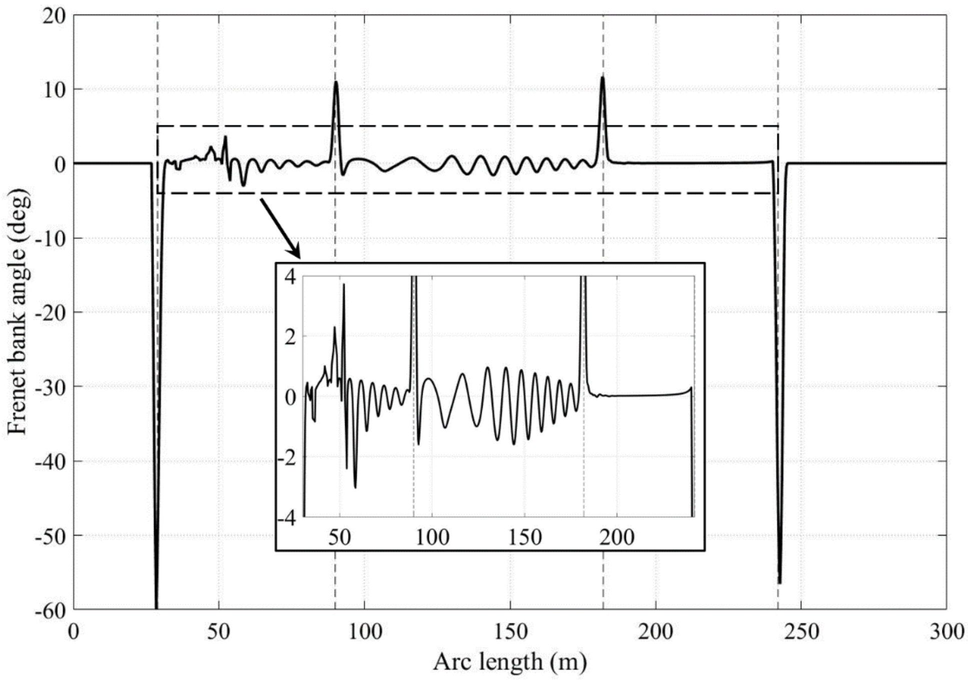

Figure 19: Frenet bank angle of the front wheelset of the three-piece bogie

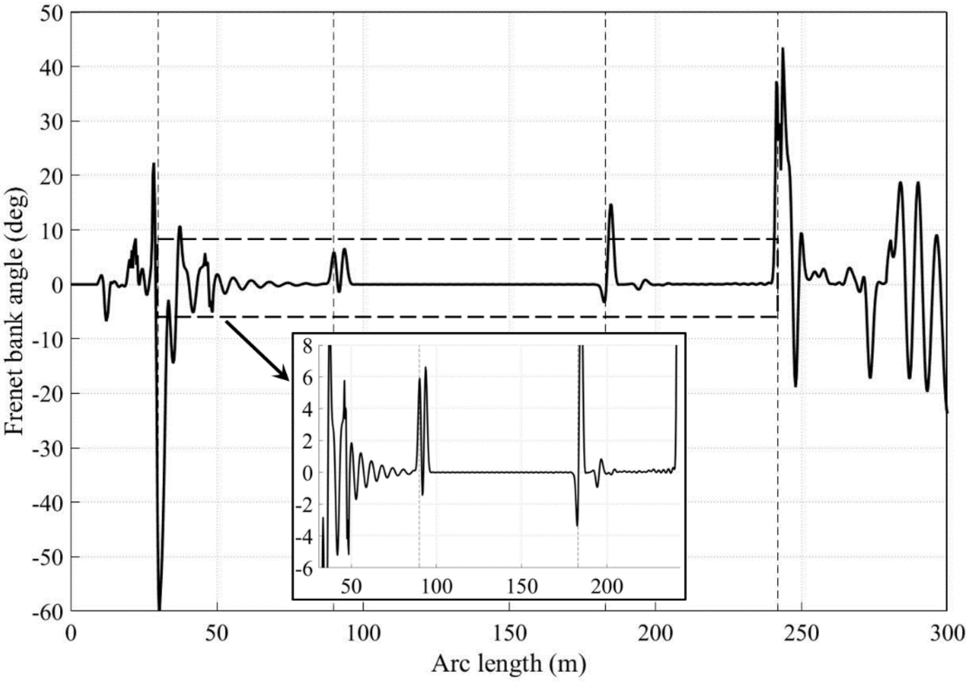

Figure 20: Frenet bank angle of the rear wheelset of the three-piece bogie

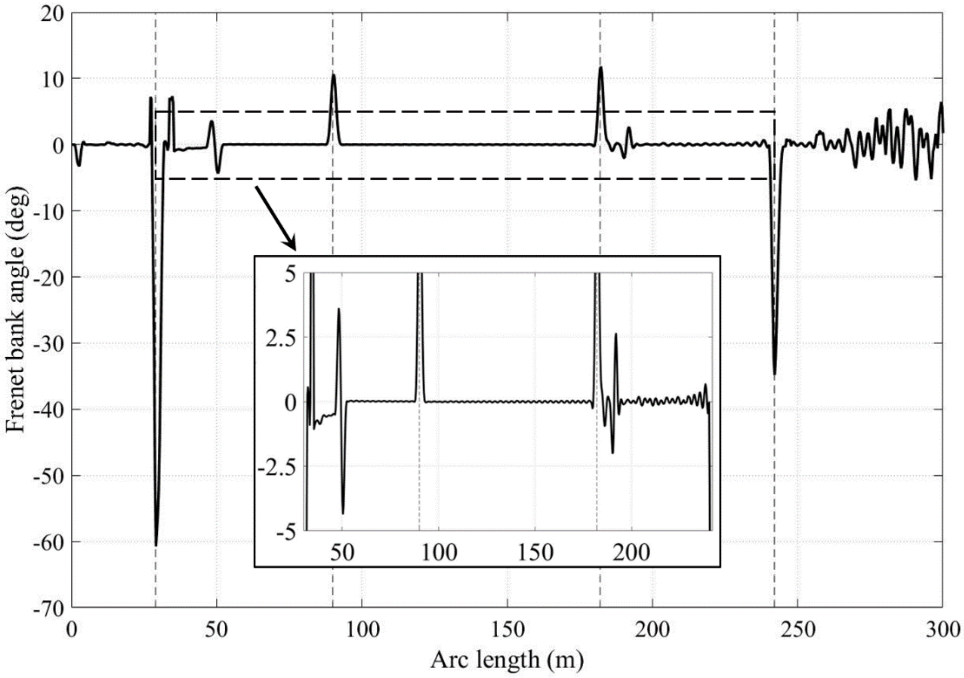

Figure 21: Frenet bank angle of the front wheelset of the Y25 bogie

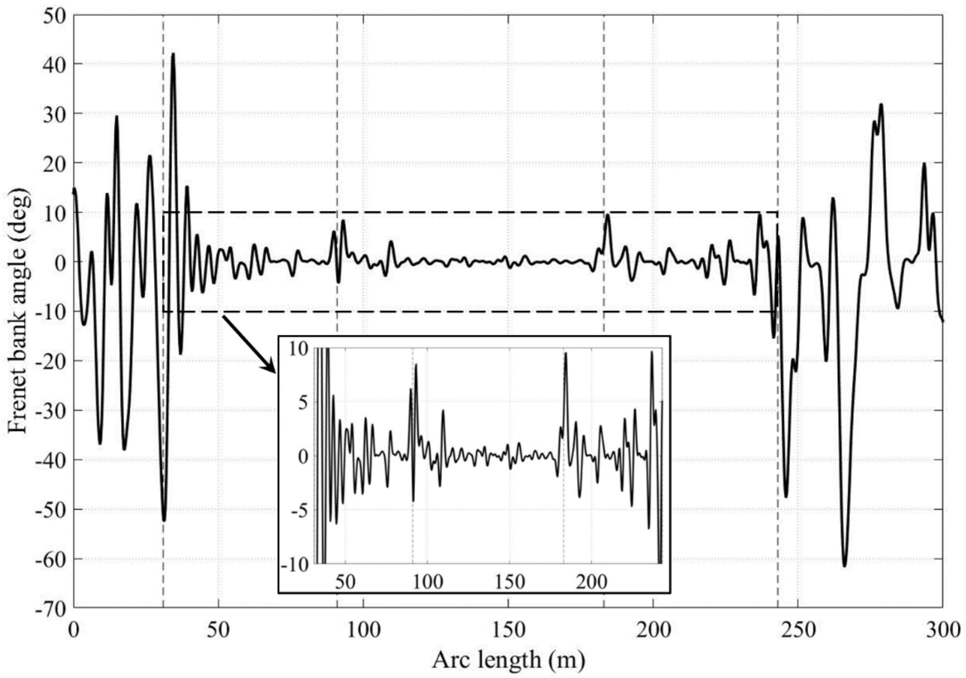

Figure 22: Frenet bank angle of the rear wheelset of the Y25 bogie

CHAPTER 10

SUMMARY AND CONCLUSIONS

A new *Frenet force analysis* integrated with a *data-driven science* (DDS) approach is proposed for the evaluation of railroad vehicle performance. Use of the new performance evaluation methodology, which is based on integrating nonlinear *multibody system* (MBS) computational algorithms and new geometric concepts, is demonstrated by comparing the performance of two widely used railroad bogies: the *three-piece bogie*, used in North America and other parts of the world, and the European *Y25 bogie*. Despite their wide use, a MBS comparative study based on Frenet force analysis is lacking in the literature. In this investigation, distinction is made between AMT curves and the track geometries. The AMT curve geometry is defined using the motion-dependent Frenet curvature and vertical development angles, which differ from their motion-independent counterparts used in the description of the track geometry. Furthermore, distinction is made between the Frenet super-elevation defined by the Frenet bank angle of AMT curves and the motion-independent track super-elevation defined by the track bank angle. The difference between the *lateral track plane force balance* used in practice to determine the balance speed and the *Frenet force balance* based on recorded motion trajectories is explained. Computer simulations of bogies travelling on a track, consisting of tangent, spiral and curve sections, are performed and the results obtained demonstrated the dependence of the AMT curve geometry on the wheelset forward motion, highlighting the limitations of tests performed using roller test rigs which do not allow longitudinal wheelset displacements.

While a judgement on the overall bogie performance cannot be made based on the results of a single investigation, the results obtained show that flange contacts occur for both the three-piece bogie wheelsets and only for the Y25 bogie front wheelset, despite performing the simulations at the balance speed. This demonstrates that the current balance speed criteria, while it lowers the impact severity, is not effective in totally eliminating the flange contact during curve negotiations. In general, the three-piece bogie front wheelset shows more stable behavior compared to the rear wheelset, while the opposite is observed for the Y25 bogie. The tendency of the Y25 bogie rear wheelset to follow the track is probably attributed to the high rigidity of the bogie frame. The flange contact force results indicate that the three-piece bogie wheels may be subjected to more flange wear due to the two-point contacts occurring for both wheelsets. It is important, however, to point out that previous investigations reported that the performance of the three-piece bogie can be worsened in the unloaded conditions (Kovalev et al, 2009; Sadeghi et al, 2011). Because all bogie performance criteria cannot be addressed in a single investigation and because of the lack of exact inertia, dimension and material data, this study was focused on specific measures without making judgement on the overall bogie performance.

CITED LITERATURE

1. Andersson, C., and Abrahamsson, T., 2002, "Simulation of Interaction between a Train in General Motion and a Track", *Vehicle System Dynamics*, Vol. 38 (6), pp. 433-455.
2. Berghuvud, A., 2002, "Freight Car Curving Performance in Braked Conditions", *IMechE Journal of Rail and Rapid Transit*, Vol. 216 (1), pp. 23-29.
3. Bettamin, D., Shabana, A., Bosso, N., Zampieri, N., 2021, "Frenet Performance Evaluation of Railroad Vehicle Systems", *Acta Mechanica*, accepted for publication.
4. Bosso, N., Gugliotta, A., and Somà, A., 2002, "Multibody Simulation of a Freight Bogie with Friction Dampers", *ASME/IEEE Joint Rail Conference*, Vol. 35936, pp. 47-56.
5. Cuenot, F., and Gabriel, C.H., 2016, "Carbon Footprint of Railway Infrastructure", *International Union of Railways.*
6. De Pater, A.D., 1988, "The Geometrical Contact between Track and Wheelset", *Vehicle System Dynamics*, Vol. 17 (3), pp. 127-140.
7. Do Carmo, M. P., 2016, *Differential Geometry of Curves and Surfaces.* Second Edition, New York: Dover Publications.
8. Dumitriu, M., 2012, "The Stationary Motion of a Bogie along a Circular Curve", *UPB Sci. Bull., Series D*, Vol. 74, pp. 39-50.
9. Elkins, J.A., and Gostling, R.J., 1977, "A General Quasi-Static Curving Theory for Railway Vehicles", *Vehicle System Dynamics*, Vol. 6 (2-3), pp. 100-106.
10. Endlicher, K.O., and Lugner, P., 1990, "Computer Simulation of the Dynamical Curving Behavior of a Railway Bogie", *Vehicle System Dynamics*, Vol. 19 (2), pp. 71-95.
11. Farin, G., 1999, *Curves and Surfaces for CAGD*, A Practical Guide, Fifth Edition, Morgan Kaufmann, Publishers, San Francisco.

CITED LITERATURE (continued)

12. Gallier, J., 2011, *Geometric Methods and Applications: For Computer Science and Engineering*, Springer, New York.
13. Ghazavi, M.R., and Taki, M., 2008, "Dynamic Simulations of the Freight Three-Piece Bogie Motion in Curve", *Vehicle System Dynamics*, Vol. 46(10), pp. 955-973.
14. Ginsberg, J., 2008, *Engineering Dynamics*, Cambridge University Press, New York.
15. Goetz, A., 1970, *Introduction to Differential Geometry*, Addison Wesley.
16. Goldstein, H., 1950, *Classical Mechanics*, Addison-Wesley.
17. Grassie, S.L., 1993, "Dynamic Modeling of the Track and their Uses. In *Rail Quality and Maintenance for Modern Railway Operation*, ed. J. J. Kalker, D. F. Cannon, and O. Orringer, pp. 165-184. Dordrecht: Kluwer.
18. Greenwood, D. T., 1988, *Principles of Dynamics*, 2nd ed., Prentice Hall, Englewood Cliffs, NJ.
19. Handoko, Y., Xia, F., and Dhanasekar, M., 2004, "Effect of Asymmetric Brake Shoe Force Application on Wagon Curving Performance", *Vehicle System Dynamics*, Vol. 41, pp. 113-122.
20. He, Y., and Mcphee, J., 2005, "Optimization of Curving Performance of Rail Vehicles", *Vehicle System Dynamics*, Vol. 43(12), pp. 895-923.
21. Huston, R. L., 1990, *Multibody Dynamics*, Butterworth-Heinemann, Stoneham, MA.
22. Hecht, M., 2001, "European Freight Vehicle Running Gear: Today's Position and Future Demands", *Proceedings of the Institution of Mechanical Engineers, Part F: Journal of Rail and Rapid Transit*, Vol. 215(1), pp. 1-11.
23. Iwnicki, S.D., Stichel, S., Orlova, A., and Hecht, M., 2015, "Dynamics of Railway Freight Vehicles", *Vehicle System Dynamics*, Vol. 53(7), pp. 995-1033.

CITED LITERATURE (continued)

24. Jalili, M. M., Motavasselolhagh, M., Fatehi, R., and Sefid, M., 2020, "Investigation of Sloshing Effects on Lateral Stability of Tank Vehicles during Turning Maneuver", *Mechanics Based Design of Structures and Machines.* doi: 10.1080/15397734.2020.1800490.
25. Jönsson, P.A., 2007, *Dynamic Vehicle-Track Interaction of European Standard Freight Wagons with Link Suspension,* Doctoral dissertation, KTH.
26. Kataori, A., Iijima, H., Momosaki, S., and Horioka, K., 2011, "Development of Continuous Measurement Equipment for Angle of Attack and Results of Measurements", *JR East Technical Review*, Vol. 19, pp. 46-49.
27. Kik, W., 1992, "Comparison of the Behavior of Different Wheelset-Track Models", *Vehicle System Dynamics*, Vol. 20 (1), pp. 325-339.
28. Knothe, K.L., and Grassie, S.L., 1993, "Modeling of Railway Track and Vehicle/Track Interaction at High Frequencies", *Vehicle System Dynamics*, Vol. 22 (3-4), pp. 209-262.
29. Knothe, K., and Stichel, S., 1994, "Direct Covariance Analysis for the Calculation of Creepages and Creep-Forces for Various Bogie on Straight Track with Random Irregularities", *Vehicle System Dynamics*, Vol. 23 (1), pp. 237-251.
30. Kreyszig, E., 1991, *Differential Geometry*, Dover Publications.
31. Kovalev, R., Lysikov, N., Mikheev, G., Pogorelov, D., Simonov, V., Yazykov, V., and Torskaya, E., 2009, "Freight Car Models and their Computer-Aided Dynamic Analysis", *Multibody System Dynamics*, Vol. 22(4), pp. 399-423.
32. Ling, H., and Shabana, A.A., 2021, "Euler Angles and Numerical Representation of the Railroad Track Geometry", *Acta Mechanica*, accepted for publication.

CITED LITERATURE (continued)

33. Pascal, J.P., and Sany, J.R., 2019, "Dynamics of an Isolated Railway Wheelset with Conformal Wheel-Rail Interactions", *Vehicle System Dynamics*, Vol. 57 (12), pp. 1947-1969.
34. Piegl, L., and Tiller, W., 1997, *The NURBS Book*, Second Edition, Springer, Berlin.
35. Rail Safety and Standards Board, 2017, "Railway Wheelsets", *Rail Safety and Standards Board Limited*.
36. Railway Technical: Vehicle Suspension Systems. http://www.railway-technical.com/archive/vehicle-suspension-systems.pdf, 2004. [Online; accessed 02/04/2021].
37. Rogers, D.F., 2001, *An Introduction to NURBS with Historical Perspective*, Academic Press, San Diego, CA.
38. Roberson, R. E., and Schwertassek, R., 1988, *Dynamics of Multibody Systems*, Springer-Verlag, Berlin.
39. Sadeghi, M., Shadfar, M., Rezvan, M., 2011, "Dynamic Modeling of Three Pieces Bogies at Curves and the Parameters Affecting its Derailment Index", *International Heavy Haul Association Conference 2011.*
40. Shabana, A.A., 2020, "*Dynamics of Multibody Systems*, Fifth Edition", *Cambridge university press,* New York.
41. Shabana, A.A., 2021, *Mathematical Foundation of Railroad Vehicle Systems: Geometry and Mechanics*, John Wiley & Sons.
42. Shabana, A.A., 2021, "Frenet Oscillations and Frenet-Euler Angles: Curvature Singularity and Motion-Trajectory Analysis", Technical Report # MBS2021-2-UIC, Department of Mechanical and Industrial Engineering, University of Illinois at Chicago.

CITED LITERATURE (continued)

43. Shabana, A.A., 2021, "Geometric Self-Centering and Force Self-Balancing of Railroad Vehicle Hunting Oscillations", *Acta Mechanica*, accepted for publication.

44. Shabana, A.A., and Ling, H., 2021, "Characterization and Quantification of Railroad Spiral-Joint Discontinuities", *Mechanics Based Design of Structures and Machines*, pp. 1-26.

45. SKF, 2011, "Railway Technical Handbook Vol. 1: Axleboxes, wheelset bearings, sensors, condition monitoring, subsystems and services", *SKF*, *Göteborg*, 2011.

46. Sun, Y.Q., and Cole, C., 2008, "Vertical Dynamic Behavior of Three-Piece Bogie Suspensions with two Types of Friction Wedge", *Multibody System Dynamics*, Vol. 19(4), pp. 365-382.

47. Technical Specialist Rolling Stock Performance Standards, 2013, "ESR 0331. Wheel and axles reference manual", *RailCorp Engineering Standard.*

48. The American Public Transportation Association, 2007, "APTA PR-M-S-015-06 Standard for Wheel Flange Angle for Passenger Equipment", *APTA PRESS Task Force*.

49. The Contact Patch: Book. https://the-contact-patch.com/book/rail, 2017. [Online; accessed 03/01/2021].

50. True, H., 1994, "Does a Critical Speed for Railroad Vehicles Exist?", *Proceedings of IEEE/ASME Joint Railroad Conference*, pp. 125-131.

VITA

NAME: Dario Bettamin

EDUCATION:

- Master of Science in "Mechanical Engineering", University of Illinois at Chicago, Chicago (USA), July 2021;
- Master's Degree in "Mechanical Engineering", Politecnico di Torino, Torino (Italy), July 2021;
- Bachelor's Degree in "Mechanical Engineering", Politecnico di Torino, Torino (Italy), September 2019.

EXPERIENCE: Research Assistant, University of Illinois at Chicago, Chicago (USA)

- Use of multibody software for dynamic simulations of rail vehicles;
- Research on numerical representation of standard rail wheel profiles.

LANGUAGES:

- Italian: Native speaker;
- English: Full professional proficiency, IELTS - C1.

PROJECTS:

- "Two Stage Speed Increaser for a Wind Power Plant", Machine Design Technical Report, Politecnico di Torino, 2020;
- "Study of a Logistic Platform (Hub) for the Distribution of Electrical Tools", Industrial Plants Project, Politecnico di Torino, 2019;
- "Road Pavement Energy Harvesting Systems", Bachelor's Thesis, Politecnico di Torino, 2019.

DIGITAL SKILLS:

- Programming Languages: Matlab, CNC ISO, Python, C;
- CAD: SolidWorks, AutoCAD;
- Simulation Software: SIGMA/SAMS, Coppelia Sim;
- Numerical-Analysis Software: Matlab, Microsoft Excel.

CONTACTS:

- E-mail: bettamin.dario@gmail.com
- LinkedIn: https://www.linkedin.com/in/dario-bettamin-a28a62210/